IVYSPRING INTERNATIONAL PUBLISHER

Theranostics

2019; 9(2): 405-423. doi: 10.7150/thno.29832

Research Paper

Delayed Remote Ischemic Preconditioning Confers Renoprotection against Septic Acute Kidney Injury via Exosomal miR-21

Tianyi Pan[1, 2*], Ping Jia[2*], Nan Chen[7, 8], Yi Fang[2], Yiran Liang[2], Man Guo[2], Xiaoqiang Ding[2, 3, 4, 5, 6]✉

1. Institutes of Biomedical Sciences, Fudan University
2. Department of Nephrology, Zhongshan Hospital, Fudan University
3. Shanghai Medical Center of Kidney
4. Shanghai Institute of Kidney and Dialysis, Shanghai, China
5. Shanghai Key Laboratory of Kidney and Blood Purification, Shanghai, China
6. Hemodialysis quality control center of Shanghai
7. Department of Cardiac Surgery, Zhongshan Hospital, Fudan University, Shanghai
8. Shanghai Institute of Cardiovascular Disease, Shanghai

*These authors contributed equally to this work

✉ Corresponding author: Xiaoqiang Ding, Address: Department of Nephrology, Zhongshan Hospital, Fudan University, 180 Feng-Lin Road, Shanghai 200032, China. Email: ding.xiaoqiang@zs-hospital.sh.cn

Received: 2018.09.10; Accepted: 2018.11.29; Published: 2019.01.01

Abstract

Sepsis is a common and life-threatening systemic disorder, often leading to acute injury of multiple organs. Here, we show that remote ischemic preconditioning (rIPC), elicited by brief episodes of ischemia and reperfusion in femoral arteries, provides protective effects against sepsis-induced acute kidney injury (AKI).

Methods: Limb rIPC was conducted on mice *in vivo* 24 h before the onset of cecal ligation and puncture (CLP), and serum exosomes derived from rIPC mice were infused into CLP-challenged recipients. *In vitro*, we extracted and identified exosomes from differentiated C2C12 cells (myotubes) subjected to hypoxia and reoxygenation (H/R) preconditioning, and the exosomes were administered to lipopolysaccharide (LPS)-treated mouse tubular epithelial cells (mTECs) or intravenously injected into CLP-challenged miR-21 knockout mice for rescue experiments.

Results: Limb rIPC protected polymicrobial septic mice from multiple organ dysfunction, systemic accumulation of inflammatory cytokines and accelerated parenchymal cell apoptosis through upregulation of miR-21 in a hypoxia-inducible factor 1α (HIF-1α)-dependent manner in the ischemic limbs of mice. However, in miR-21 knockout mice or mice that received HIF-1α siRNA injection into hind limb muscles, the organ protection conferred by limb rIPC was abolished. Mechanistically, we discovered that miR-21 was transported from preischemic limbs to remote organs via serum exosomes. In kidneys, the enhanced exosomal miR-21 derived from cultured myotubes with H/R or the serum of mice treated with rIPC integrated into renal tubular epithelial cells and then targeted the downstream PDCD4/NF-κB and PTEN/AKT pathways, exerting anti-inflammatory and anti-apoptotic effects and consequently attenuating sepsis-induced renal injury both *in vivo* and *in vitro*.

Conclusion: This study demonstrates a critical role for exosomal miR-21 in renoprotection conferred by limb rIPC against sepsis and suggests that rIPC and exosomes might serve as the possible therapeutic strategies for sepsis-induced kidney injury.

Key words: remote ischemic preconditioning, miR-21, sepsis, acute kidney injury, exosomes

Introduction

Sepsis, a systemic disorder secondary to a life-threatening infection, is characterized by initial hyperinflammaion, protracted host immunosuppression and multiple organ dysfunction. Sepsis-induced acute kidney injury (septic AKI), accompanied by multiple organ dysfunction, contributes to the high mortality in intensive care units (ICUs) [1-3]. Previous studies of septic AKI have focused on solutions to systemic hypotension, and currently, the consensus opinion is that tubular injury plays a pivotal role in progression of the disorder [4, 5]. Although septic AKI has been extensively studied, major advancements in anti-inflammatory and anti-apoptotic mechanisms indicate the need for further investigation.

Remote ischemic preconditioning (rIPC), a beneficial stimulus triggered by short episodes of ischemia and reperfusion (I/R) in remote tissues, was initially applied for cardiac protection [6]. Growing evidence has shown that the beneficial effects of rIPC can be observed in multiple organs with subsequent ischemic injury [7]. In renoprotection, rIPC is a practical method for reducing the incidence of AKI among patients after cardiac surgery [8]. Although previous data provide a better understanding of rIPC, the underlying mechanism of its modulation in remote tissues remains unknown. A series of humoral factors might constitute the protective mechanism of rIPC [9-11]. Cai et al. demonstrated that plasma IL-10 can be upregulated by rIPC for cardiac protection via activation of hypoxia-inducible factor 1α (HIF-1α) [12]. In addition to its role as a direct cytomediator, the effect of rIPC on modulating noncoding RNA expression has been reported, suggesting a novel mechanism through which rIPC exerts its effects [13,14].

MicroRNAs (miRNAs) are small RNAs that exert pleiotropic effects in multiple pathological processes, including regulation of inflammation and cell apoptosis [15]. Moreover, the transport of miRNAs has drawn wide attention because miRNAs are more stable in circulation [16,17]. Recent studies have implicated IPC (ischemic preconditioning; a stimulus is conducted on parenchymal organs, which subsequently experience long-term ischemic injury) as an important factor influencing miRNA expression [18-20], such as the variation in miR-21 levels post-IPC [21-22]. Our previous study showed that the miR-21 expression level increases after renal IPC and that its high expression protects kidneys from lipopolysaccharide (LPS)-induced injury [20]. We conducted the present study to 1) investigate whether limb rIPC, a modified preconditioning strategy conducted on bilateral femoral arteries, could upregulate the systemic miR-21 level to inhibit multiorgan injury, specifically, septic AKI and 2) to clarify the potential mechanism underlying the protective effect of limb rIPC against sepsis-induced injury.

In this study, we hypothesized that limb rIPC could ameliorate renal dysfunction in a mouse model of polymicrobial sepsis through crosstalk between skeletal muscles and kidneys by transferring exosomal miR-21 to the circulation. Elevated miR-21, originating from preconditioned limbs and possibly shuttled to the kidneys by circulating exosomes, suppressed systemic inflammation and renal tubular cell apoptosis. In addition, infusion of exosomes derived from myotubes cultured under hypoxia and reperfusion preconditioning or serum from rIPC-treated mice into miR-21$^{-/-}$ or wild-type mice provided renoprotection against sepsis. Our research may provide a potential therapeutic modality for sepsis-associated AKI.

Results

Limb rIPC protects against multi-organ injury in sepsis

Using a mouse model of cecal ligation and puncture (CLP), we evaluated the effects of limb rIPC on multiorgan injury induced by sepsis. The interval between rIPC and CLP was 24 h. Compared with the CLP group, limb rIPC clearly relieved the kidney, liver and lung dysfunction, evidenced by the significant decrease in the level of serum creatinine (SCr), NGAL expression, alanine transaminase (ALT) and pulmonary edema formation (**Figure 1A-D**). During the seven days post preconditioning, rIPC improved the survival rate of mice challenged by CLP (**Figure 1E**). Accordingly, limb rIPC ameliorated the histological damage in mice challenged by 24 h CLP injury. In kidneys, alleviation of partial tubular vacuolization, brush border loss and inflammatory cell infiltration was observed in the outer strip of the outer medulla [23]. In the liver, the level of hepatocyte vacuolization was reduced with limb rIPC. We also observed that the CLP challenge accelerated lung injury, and limb rIPC significantly reduced the formation of edema and neutrophil infiltration in the tissue (**Figure 1F-G**).

Limb rIPC reduces inflammation and apoptosis in mice subjected to CLP

Serum tumor necrosis factor (TNF-α) and interleukin 6 (IL-6) concentrations and their levels in the kidneys were analyzed, and elevation of these cytokines was primarily observed 24 h after CLP. rIPC significantly blocked elevation of these cytokines in the serum and kidneys (**Figure 2A-D**). Consistently, limb rIPC blocked the increase in IL-6 mRNA in the

lung and liver caused by the CLP challenge (**Figure S1A-B**). Furthermore, neutrophil or monocyte infiltration into the kidney was clearly shown by myeloperoxidase (MPO) staining. MPO levels were prominent at 24 h post-CLP in the interstitial area of the kidney (**Figure 2E-F**), and limb rIPC efficiently reduced the CLP-induced inflammatory cell infiltration. In the lung and liver, quantification of MPO-positive cells showed a reduction in the rIPC+CLP group compared with the CLP-challenged group (**Figure S1C-D**).

Terminal deoxynucleotidyl transferase dUTP nick-end labeling (TUNEL) was used to detect apoptotic cells in the kidney. Limb rIPC significantly reduced the number of apoptotic cells in the kidney 24 h after CLP (**Figure 2F**). In addition, the levels of cleaved caspase-3 and BCL-2, both key mediators of cell apoptosis, were measured. Limb rIPC suppressed the increase in cleaved-caspase3 protein levels and increased BCL-2 protein levels, thereby attenuating the apoptotic effect induced by CLP (**Figure 2G-H**). In the lungs but not in the liver, limb rIPC also suppressed the increase in cleaved-caspase3 protein induced by CLP challenge (**Figure S1E-F**).

Additionally, we examined the ability of limb rIPC to attenuate renal dysfunction and the effect of anti-inflammatory cytokine production in mice challenged by LPS administration (20 mg/kg). Compared with the LPS group, mice in the rIPC+LPS group showed a reduced level of serum creatinine and decreased IL-6 and TNF-α serum concentrations (24 h after LPS administration) (**Figure 3A-C**). In addition, cast formation, tubular cell vacuolization and loss of brush border was observed in the outer stripe of the outer medulla in kidneys with LPS administration. In contrast, mice with limb rIPC before LPS treatment showed mild morphologic changes (**Figure 3D**).

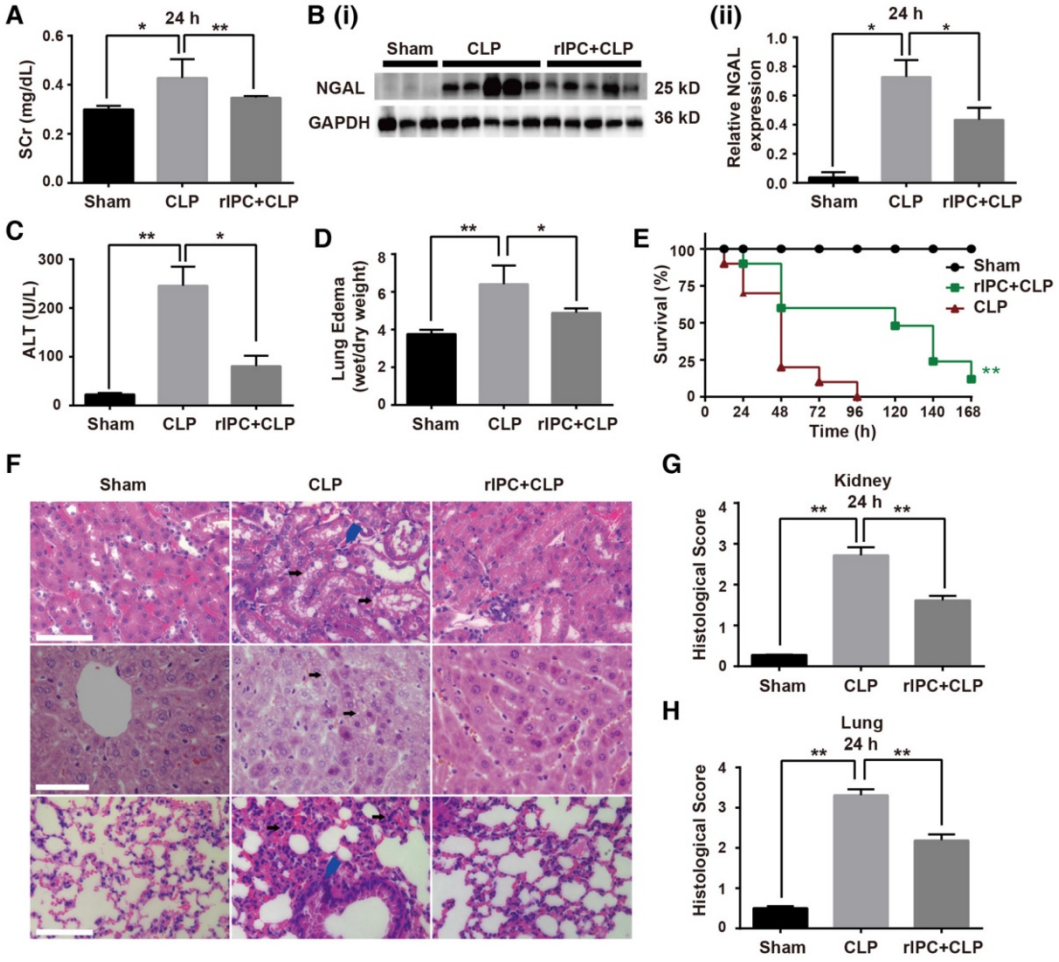

Figure 1. Limb remote ischemic preconditioning ameliorates sepsis-induced acute organ injury. Mice received short episodes of ischemia and reperfusion in the bilateral limbs 24 h before CLP. **(A)** Serum creatinine (SCr) was measured (n = 6, in each group). **(B)** Immunoblot analysis of neutrophil gelatinase-associated lipocalin (NGAL) expression in the kidney was tested (sham: n = 3, CLP: n = 5, rIPC+CLP: n = 5). **(C)** Serum alanine transaminase (ALT) was evaluated (n = 6, in each group). **(D)** Edema formation in the lung determined by calculation of the wet/dry ratio (n = 6, in each group). **(E)** The survival rate of mice after CLP injury with rIPC treatment (n = 10, in each group). **(F-G)** Morphological changes in the kidney, liver and lung and quantification of histological damage in the kidney and lung. Tissue sections were stained with hematoxylin and eosin (HE) (scale bar: 25 μm); black arrow in the kidney and liver images indicates cell vacuolization; blue arrow indicates inflammatory cell infiltration) (n = 5, in each group). *p < 0.05, and **p < 0.01. The data are presented as the mean ± SEM. Each experiment was replicated more than three times.

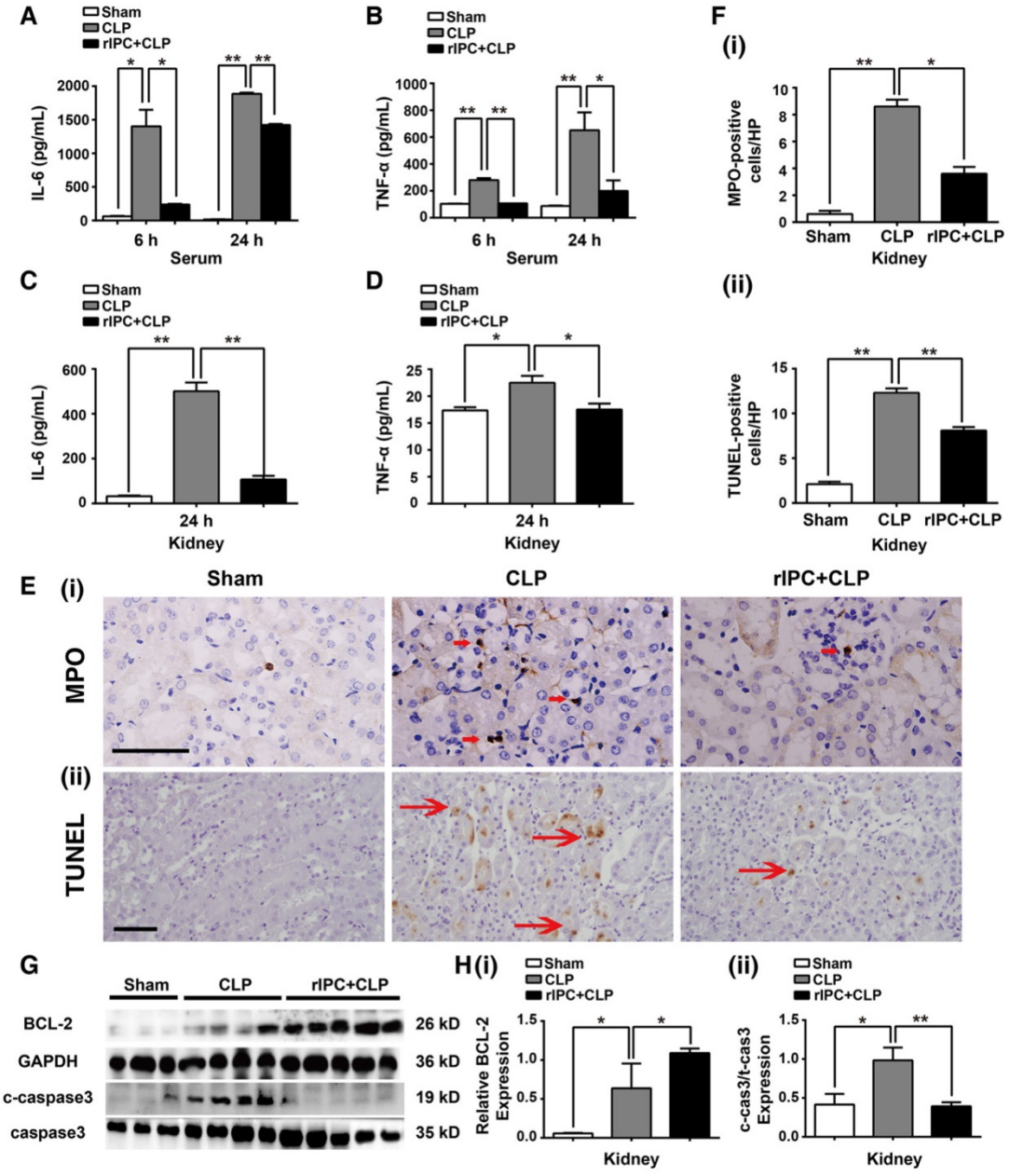

Figure 2. Limb rIPC reduced inflammation and apoptosis in CLP-challenged mice. (A-B) Enzyme-linked immunosorbent assay (ELISA) of interleukin (IL)-6 and tumor necrosis factor (TNF)-α in serum in different groups at 6 or 24 h. **(C-D)** ELISA of IL-6 and TNF-α in kidneys at 24 h in different groups. **(E)** Myeloperoxidase (MPO)-positive staining for inflammatory cell infiltration in renal sections (scale bar, 25 μm). **(F)** Terminal deoxynucleotidyl transferase-mediated dUTP nick-end labeling (TUNEL)-positive cells in renal sections (scale bar, 50 μm). **(G-I)** Immunoblot analysis of B-cell lymphoma (BCL)-2 and cleaved caspase-3 (c-caspase3) protein expression in kidneys 24 h after CLP with limb rIPC. Limb rIPC upregulated BCL-2 and downregulated c-caspase3 expression. (n = 4, or n = 6). *$p < 0.05$, and **$p < 0.01$. The data are presented as the mean ± SEM.

Kidney protection by rIPC is abolished in miR-21$^{-/-}$ mice

MiR-21, an anti-apoptotic miRNA, was found to be elevated in the kidneys and lungs after limb rIPC treatment (**Figure 4A**). The limb skeletal muscle, which is anatomically adjacent to the femoral arteries subjected to ICP, might be the origin of the miR-21 released into the circulation. Indeed, we found that limb rIPC stimulated miR-21 levels in the muscles 24 h after treatment (**Figure 4A**). To observe the precise distribution of miR-21, miR-21 levels in murine skeletal muscles, kidneys, lungs and livers were measured at different time points (0, 2, 6, 12 and 24 h) after rIPC. Although a small peak at 2 h and a slight decrease at 6 h were observed post-rIPC in multiple organs, limb rIPC was associated with a progressive increase in miR-21 levels during the period (**Figure 4B**). Pre-miR-21, the precursor miRNA product, can be delivered by the enzyme exportin 5 into cytoplasm and further processed into mature miR-21 by another enzyme. Here, the expression of pre-miR-21 in

skeletal muscles and kidney was evaluated, and we found that the pre-miR-21 level was significantly upregulated in the muscles but was not increased in the kidney (**Figure 4C**). These results suggest that the miR-21 gene might be transcribed in the skeletal muscles of the limbs that had been subjected to short periods of ischemia and reperfusion.

To validate the protective role of miR-21 in septic injury, we utilized a miR-21 knockout (miR21$^{-/-}$) mouse model and concentrated on renal modulation post-rIPC. These mice and their wild-type (WT) littermates were subjected to limb rIPC 24 h before the onset of CLP. As shown in **Figure 4D-E**, limb rIPC was unable to suppress the elevations in SCr and NGAL expression in the kidneys of the CLP-challenged miR21$^{-/-}$ mice. Moreover, enzyme-linked immunosorbent assays (ELISA) and MPO staining revealed that preconditioning did not attenuate the damage to CLP-challenged miR21$^{-/-}$ mouse kidneys, such as the increase in pro-inflammatory cytokine production and inflammatory cell infiltration. Accordingly, miR-21 silencing significantly suppressed the anti-apoptotic effects that were evoked by limb rIPC, evidenced by the increased number of apoptotic cells detected in miR-21$^{-/-}$ mice via TUNEL assay (**Figure 4F-I**).

Inhibition of HIF-1α abrogates renoprotection induced by rIPC in mice

HIF-1α plays an essential role in response to hypoxia conditions. Studies have shown that, HIF-1α, a transcription factor, participates in transcription regulation, including miRNA expression [49,50]. Among hypoxia-related miRNAs, the feedback loop between miR-21 and HIF-1α has been well established in various pathophysiological processes [24]. Our experiments showed that HIF-1α expression was significantly elevated in the muscles at 24 h post rIPC (**Figure 5A-B**). However, HIF-1α expression in remote organs was not altered (**Figure 5C**). To evaluate the effect of HIF-1α on renoprotection induced by limb rIPC against sepsis, 10 μg HIF-1α siRNA was introduced 2 h before rIPC to knockdown HIF-1α expression in murine skeletal muscles. Application of the siRNA efficiently inhibited HIF-1α protein and mRNA expression compared with the control group (NC/rIPC) (**Figure 5D-E**). Correspondingly, the elevated miR-21 level in skeletal muscle in response to rIPC decreased by more than 60% when HIF-1α was inhibited, and in the kidney, a 50% reduction was observed (**Figure 5F-G**). Furthermore, inhibition of HIF-1α in preconditioned skeletal muscles reduced the renal protective effect of rIPC against septic injury, and the levels of serum creatinine, NGAL expression and ALT rebounded in the HIF-1α siRNA/rIPC+CLP group compared with those in the NC/rIPC+CLP group (**Figure 5H-I**). As shown in **Figure 5J-L** and **Figure S2**, when blocking the HIF-1α expression in skeletal muscles, even with limb rIPC preconditionning, enhanced inflammatory cytokine expression in the kidney, upregulation of c-caspase3 proteins in the kidney and accelerated inflammatory cell infiltration in multiple organs were detected after CLP challenge.

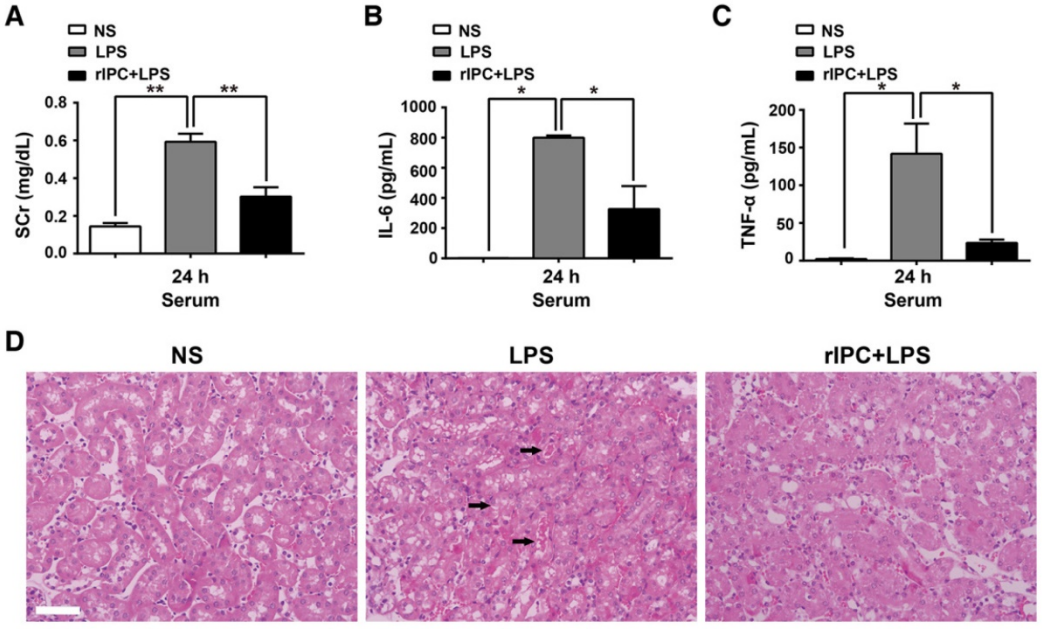

Figure 3. Limb rIPC ameliorates LPS-induced acute kidney injury. Mice received short episodes of ischemia and reperfusion in the bilateral limbs 24 h before lipopolysaccharide (LPS) administration (20 mg/kg). **(A-C)** Serum creatinine and serum pro-inflammatory cytokine concentrations were analyzed in LPS-challenged mice with or without limb rIPC. (n = 4, or n = 6). **(D)** Morphological changes in the kidney. Kidney sections were stained with hematoxylin and eosin (HE) (scale bar, 50 μm); black arrow indicates cell vacuolization or cast formation). *p < 0.05, and **p < 0.01. The data are presented as the mean ± SEM.

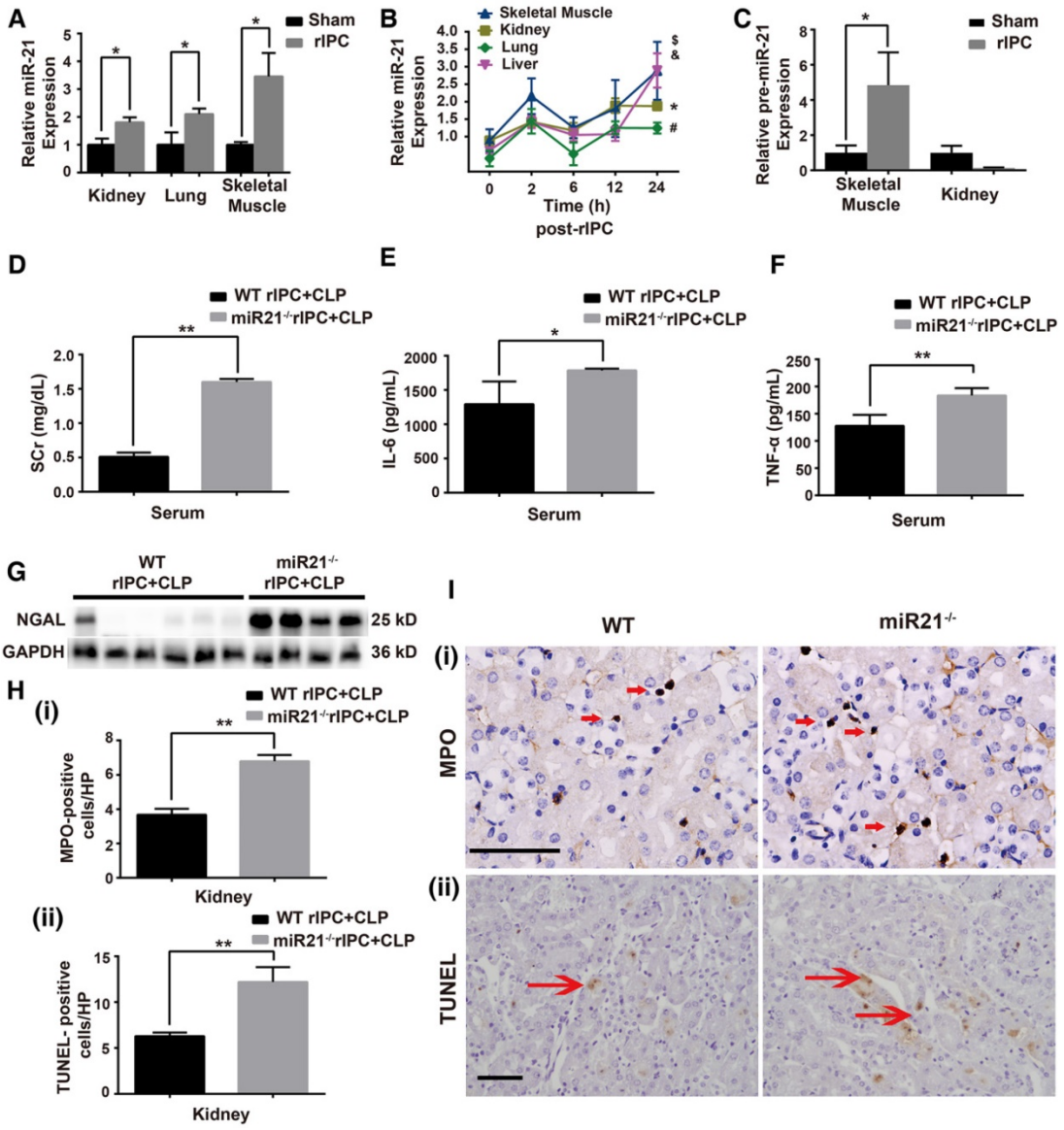

Figure 4. MiR-21 knockout abrogates the renal protection conferred by limb rIPC. Mice in the limb rIPC group were preconditioned with 4 cycles of clamping for 5 min and unclamping for 5 min in the bilateral femoral arteries. **(A)** miR-21 expression was elevated after 24 h in the kidneys, lungs and skeletal muscles of mice that received limb rIPC compared with the sham group mice (who underwent all surgical procedures except femoral artery clamping) (n = 4). **(B)** miR-21 expression in the skeletal muscles, kidneys, lungs and livers of mice at different time points (n = 4). **(C)** Pre-miR-21 expression in skeletal muscles and kidneys; the expression of the precursor miRNA product was significantly increased in skeletal muscles with limb rIPC but showed no significant change in the kidney (n = 4). **(D-I)** miR-21$^{-/-}$ mice and their wild-type littermates were subjected to limb rIPC and subsequent CLP challenge; the interval was 24 h. Renal function, inflammation and apoptosis were analyzed. (D-E) miR-21 knockout increased the serum creatinine and NGAL levels (n ≥ 4). (F-G) Enzyme-linked immunosorbent assay of IL-6 and TNF-α production in serum. H and I, Kidney sections were stained for MPO to assess the number of infiltrated inflammatory cells in kidney sections (scale bar, 25 μm). The mean number of MPO-positive cells in renal sections was analyzed. TUNEL staining was performed to examine apoptotic cells (scale bar, 50 μm). The mean number of TUNEL-positive cells in renal sections was calculated. *p < 0.05, and **p < 0.01. The data are presented as the mean ± SEM.

Exosomes function as carriers that transport miR-21 from ischemic limbs to the kidneys

As mentioned above, increased miR-21 levels were detected without HIF-1α upregulation in remote organs. We hypothesized that the higher expression of miR-21 in circulation originated from preconditioning of skeletal muscles and miR-21 might be transported to distal tissues via a specific carrier. Extracellular vesicles (EVs) that contain diverse cargoes (proteins, RNA, DNA, and lipids) have emerged as a crosstalk factor in cell-cell communication. In the present study, the double-layered nature of the vesicles, extracted from murine or human serum, was observed by transmission electron microscopy (TEM) (**Figure 6A** and **Figure S3A**). Then, the results of a nanoparticle tracking system by Dynamic Light Scattering assay revealed that the diameters of the vesicles were within 15-150 nm and, among them, the vesicles with 88.26 nm occupied the majority. Particle dispersion index (PDI) of the isolated vesicles was 0.402. Moreover, flow cytometry and western

blotting analysis detected exosome markers, such as CD63 or CD81 (**Figure 6B** and **Figure S3B**). Finally, we measured the levels of miR-21 in the exosomes at different time points (0, 2, 6, 12 and 24 h) after rIPC. We found that the miR-21 content in murine serum was upregulated 2 h post-rIPC and was stable for 24 h (**Figure 6C**). Notably, exosomal miR-21 expression in human serum samples showed a gradual increase from 2 h to 24 h after rIPC (**Figure 6D**).

To evaluate whether exosomes could be taken up by target cells, we used murine myotubes differentiated from murine C2C12 cells. The morphology of exosomes obtained from the supernatants of cultured myotubes that were subjected to hypoxia for 6 or 24 h followed by 4 h of reoxygenation treatment (hypoxia and reoxygenation [H/R]), was identified by TEM. The presence of the exosome marker CD63 was confirmed by western blotting (**Figure S3C-D**). Abundant miR-21 was found in the 24 h H/R myotubes and their exosomes (**Figure 6E** and **Figure S3E**). As shown in **Figure S3F**, the abundance of miR-21 might be associated with the HIF-1α elevation in myotubes with H/R pretreatment. In addition, the serum exosomal miR-21 level significantly decreased when mice were treated with HIF-1α siRNA prior to rIPC (**Figure S3G**). Internalization of exosomes derived from H/R myotubes, which were labeled with PKH26 dye, by mouse renal tubular epithelial cells (mTECs) was detected with a confocal microscopy assay (**Figure 6F**). Moreover, we observed that myogenin, a muscle-specific promyogenic factor [62], was obviously expressed in serum exosomes from mice with limb rIPC compared with the slight expression in serum exosomes from sham-treated mice (**Figure 6G**). The results suggest the origination of functional circulating exosomes.

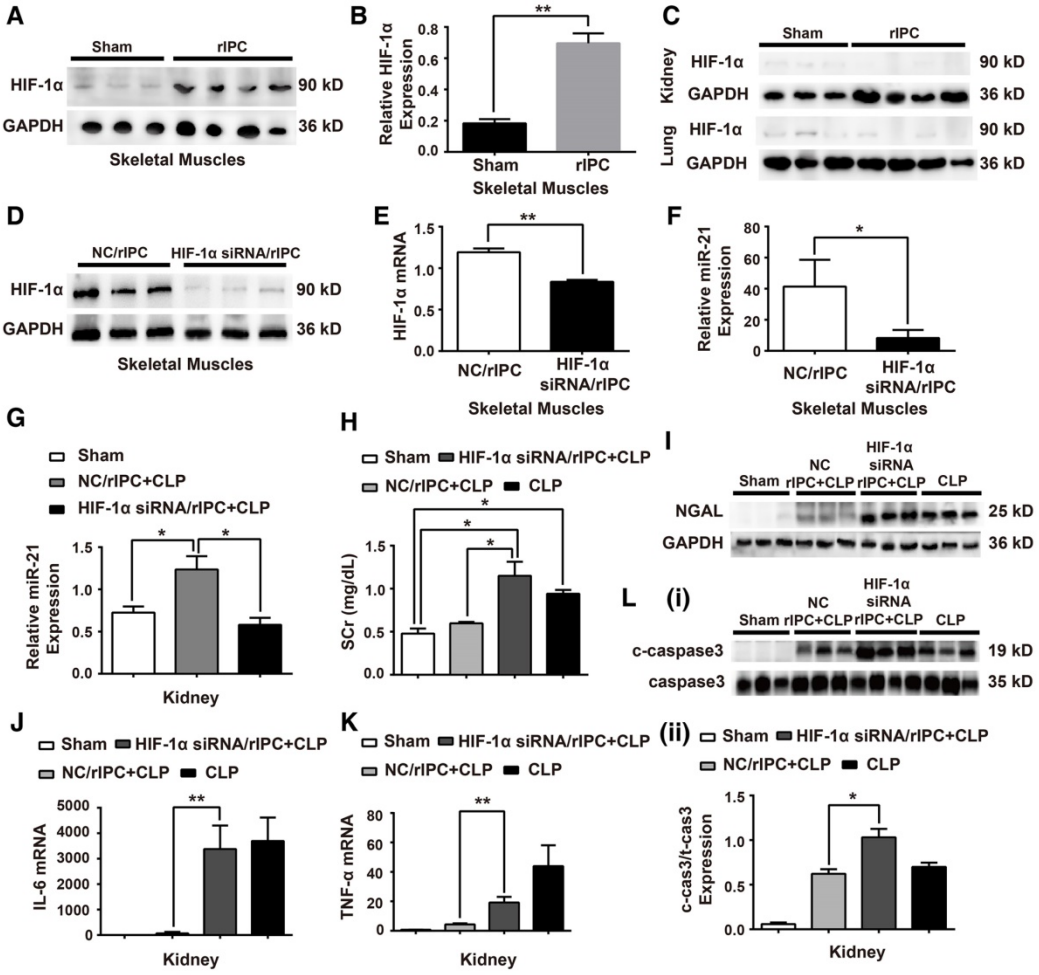

Figure 5. Knockdown of HIF-1α in skeletal muscles abolishes the systemic miR-21 expression and renal protective effect induced by rIPC. (A-B) Immunoblot analysis of HIF-1α protein in skeletal muscles. HIF-1α expression was parallel to the miR-21 level and enhanced with limb rIPC. (n ≥ 3). **(C)** Immunoblot analysis of HIF-1α protein in the kidneys and lungs. There was no significant difference between the sham and rIPC groups. (n ≥ 3). **(D-F)** HIF-1α siRNA (10 μg) was injected into skeletal muscles 2 h prior to rIPC to knockdown of HIF-1α expression. A negative control (NC) was used in the control group. (D-E) Immunoblot analysis of HIF-1α protein expression and qPCR assay of HIF-1α mRNA levels in skeletal muscles (n ≥ 3). (F) qPCR assay of miR-21 expression in skeletal muscles using HIF-1α siRNA or NC prior to rIPC. (n ≥ 4). **(G)** qPCR assay of miR-21 expression in the kidney after HIF-1α siRNA or NC treatment prior to rIPC (n ≥ 4). **(H-I)** Evaluation of the Scr level and NGAL expression in kidneys after treatment with HIF-1α siRNA or NC (n ≥ 4). **(J-K)** mRNA levels of pro-inflammatory cytokines in the kidney were measured via qPCR (n ≥ 4). **(L)** Apoptosis-related protein expression in kidneys was measured via immunoblot analysis (n ≥ 3). *p < 0.05, and **p < 0.01. The data are presented as the mean ± SEM.

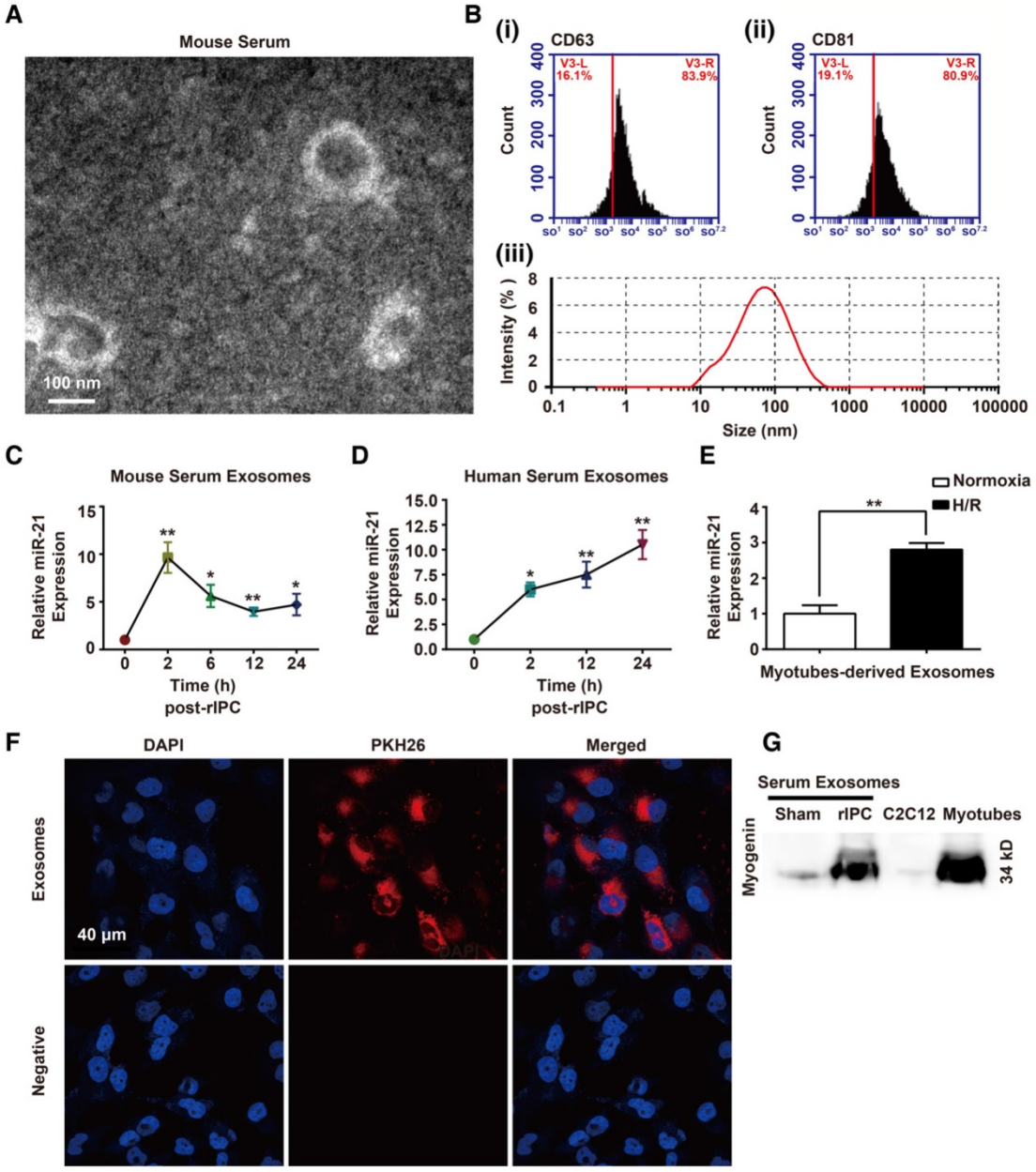

Figure 6. Identification of exosomes and analysis of the exosomal miR-21 content. (A-B) Morphological analysis of serum exosomes from mice. (A) Electron micrograph showing the diameter of the small particles collected from mouse serum post rIPC. Scale bar, 100 nm. (B) Characterization of exosomes via analysis of the expression of the mouse serum exosomal markers CD63 and CD81 via flow cytometry. A nanoparticle trafficking system (NTA) was used to analyze the sizes and concentrations of the mouse serum exosomes. According to the NTA, the particle sizes ranged between 15 and 150 nm, and the principle peak size of the particles was 88.26 nm. Particle dispersion index (PDI) of the isolated particles was 0.402. (n = 3). **(C-D)** miR-21 expression in the exosomes from mouse or human serum at different time points post rIPC based on qPCR (n = 4). **(E)** miR-21 expression in myotubes (under hypoxia and reoxygenation or normoxia) was measured via qPCR (n = 4). **(F)** Myotube (under hypoxia and reoxygenation)-derived exosomes labeled with PKH-26 dye were internalized by mouse renal tubule epithelial cells (mTECs). The nuclei of mTECs were stained with DAPI. (Scale bar, 40 μm). **(G)** Myogenin, a muscle-specific promyogenic factor, was analyzed by immunoblot assay, and expression of the protein was significantly increased in serum exosomes after rIPC (myogenin expression in C2C12 cells and in myotubes were set as the negative and positive controls, respectively). *p < 0.05, and **p < 0.01. The data are presented as the mean ± SEM.

Infusion with exosomes derived from hypoxia-pretreated myotubes attenuates sepsis-associated renal injury

To analyze the function of H/R myotube-derived exosomal miR-21 in an *in vitro* sepsis model, mTECs were treated with LPS (100 ng/mL) (**Figure S4**), and we measured the IL-6 levels in mTEC supernatants, the expression of apoptosis-related proteins and the cell apoptosis ratio. The protection effect mediated by the exosomes was observed in mTECs against LPS challenge (**Figure 7A-E**). A loss-of-function analysis was performed *in vitro* using LNA anti-miR-21 (100 nM) (**Figure 7F**). The anti-inflammatory function was blocked when miR-21 in exosomes from myotubes was suppressed, shown by the elevated IL-6 concentration in the supernatants of

mTECs (**Figure 7G**). As shown in **Figure 7H-I**, the level of cleaved caspase-3 that rebounded after miR-21 was knocked down in the myotube-derived exosomes, but the expression of BCL-2 was significantly downregulated. Additionally, the exosomes with miR-21 knockdown were unable to reduce the LPS-induced apoptosis of mTECs (**Figure 7J-K**).

Our data suggest that miR-21 delivered by exosomes protects the renal tubules from severe injury. For future translational endeavors, we examined the biodistribution of the exosomes derived from H/R myotubes in the circulation of mice without injury and mice challenged by CLP. The exosomes from H/R myotubes, labeled with DiR dye, were intravenously injected into WT mice in the sham group and monitored with an imaging system over 24 h. As shown in **Figure 8A**, with mice in the lateral position, fluorescence signals were clearly observed in the lung at 2 h postinjection. The signals gradually migrated to other parenchymal organs and accumulated in the kidney at 6 h postinjection. Until 24 h postinjection, the exosomes with DiR dye maintained stable signals in these organs. In addition, ex vivo imaging of the major organs at 24 h confirmed the presence of exosomes in the lungs, liver and kidneys but only low levels were detected in the heart (**Figure 8B**). Meanwhile, as shown in **Figure 8A**, signals were also observed in mice in both the supine position and prone position at different time points postinjection. Furthermore, the fluorescence signals were tracked in miR-21$^{-/-}$ mice and their WT litter mates challenged by CLP for different exposure times. The signals were detected at 6 h postinjection, especially in the kidney and were enhanced at 24 h (**Figure 8C**).

To assess whether exosomes derived from H/R myotubes could protect organ function in miR-21$^{-/-}$ mice with CLP injury, exogenous exosomes were intravenously injected into miR-21$^{-/-}$ mice immediately after CLP. Initially, 6 h post injection, we observed accumulation of the exosomes labeled with PKH26 dye (red staining) in the renal epithelial cells of miR-21$^{-/-}$ mice challenged by CLP, and the renal cells were characterized by Aquaporin 1 labeling (AQP1, green staining), a marker for renal tubular epithelium (**Figure 9A**). In addition, the mice treated with exosomes immediately after CLP showed reduced Scr levels, NGAL protein expression, ALT levels and lung edema formation compared with mice in the phosphate-buffered saline (PBS)-injection group (**Figure 9B-D**). As shown in **Figure 9E-F**, the concentrations of pro-inflammatory cytokines were decreased in CLP-miR-21$^{-/-}$ mice injected with exosomes from H/R myotubes compared with those in mice injected with PBS. Meanwhile, there was a lower number of MPO-positive cells in the kidneys, lungs and livers from CLP-miR-21$^{-/-}$ mice given the exosome injection (**Figure S5**). In addition, lower apoptosis-related protein expression in the kidney was detected in CLP-miR-21$^{-/-}$ mice following injection of H/R myotube-derived exosomes (**Figure 9G**). Moreover, we observed the level of HIF-1α in skeletal muscles and miR-21 expression in kidneys from mice 24, 72 and 120 h after rIPC and CLP challenge. As shown in **Figure S6A-B**, compared with the sham group, rIPC obviously promoted HIF-1α expression in the skeletal muscles after 24 and 72 h, whereas almost no HIF-1α expression was observed in the muscles after 120 h. Accordingly, the miR-21 level in the kidneys did not decline until 120 h post rIPC+CLP (**Figure S6C**). Combined with the survival rate data, these results suggest that the high level of miR-21 in remote organs in response to the increased HIF-1α expression in skeletal muscles induced by rIPC is essential for organ protection and subsequently improved the survival rate against sepsis.

miR-21 regulates signaling of its target PDCD4/NF-κB and PTEN/AKT pathways in the kidney

In vivo, limb rIPC inhibited the elevation in PDCD4 protein levels and further decreased the activation of NF-κB in the kidneys induced by CLP challenge. The alterations in PTEN levels in the kidney were consistent with the variations in PDCD4 expression in the different groups (**Figure 10A-B**). Furthermore, after systemic elimination of miR-21, limb rIPC was unable to suppress the PDCD4 expression, NF-κB activity or PTEN expression induced by CLP (**Figure 10C-D**). The levels of miR-21-targeted genes and their downstream signaling pathways were analyzed *in vitro*. LPS treatment upregulated PDCD4 and PTEN levels, further inhibited AKT phosphorylation and stimulated phospho-P65 in mouse renal tubular epithelial cells. PDCD-4/NF-κB pathway and PTEN signaling were inhibited by preadministration of myotube-derived exosomes in mTECs. (**Figure 10E-F**). Preadministration of myotube-derived exosomes with LNA anti-miR-21 (100 nM) failed to efficiently suppress these targets in mTECs compared with cells treated with the anti-scramble construct after LPS treatment (**Figure 10G-H**).

Infusion with serum exosomes derived from rIPC-treated mice protects recipient mice from CLP injury

A study was performed to determine whether circulating exosomes derived from rIPC-treated mice

(r-EXO) have therapeutic effects in CLP-challenged mice. As shown in **Figure 11A**, compared with mice given an I.V. injection of exosomes derived from sham mice (S-EXO) or mice treated with normal saline (NS), mice injected with r-EXO (200 μg in 100 μL NS) showed an increased miR-21 expression level. Then, autologous r-EXO, S-EXO or NS were administered via I.V. injection to mice immediately after CLP execution. rIPC-treated serum exosomes improved renal function by inhibiting the increase in serum creatinine and the expression of NGAL protein in CLP-challenged mice (**Figure 11B-C**). Meanwhile, an improvement in liver and pulmonary function was detected in r-EXO-injected CLP mice, evidenced by the decline in ALT level and the alleviation of lung edema (**Figure 11D-E**). r-EXO injection also significantly reduced the level of IL-6 mRNA and downregulated the expression of c-caspase3 in the kidneys (**Figure 11F-G**). According to the upregulated renal miR-21 level, the downstream signaling protein (PDCD-4 and PTEN) levels slightly declined in the kidneys of the r-EXO-injected mice (**Figure 11G**). The results suggest a potent therapeutic effect of exosomes from rIPC serum against sepsis.

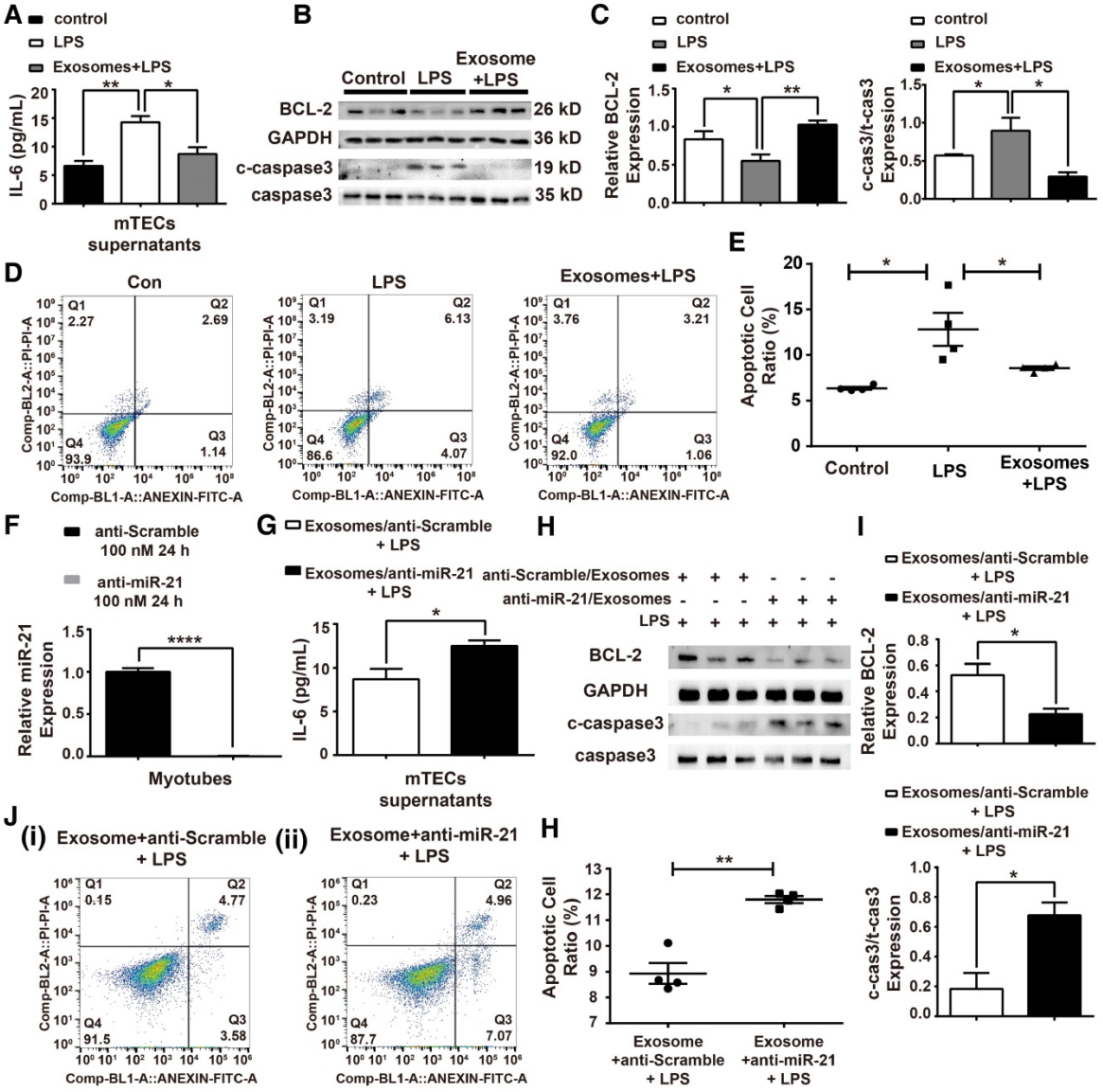

Figure 7. Myotube-derived exosomes protect mTECs from LPS-induced injury via miR-21 elevation. (A-E) Prior to LPS (100 ng/mL) challenge, mTECs were administered with exosomes derived from H/R myotubes. (A) Enzyme-linked immunosorbent assay of interleukin (IL)-6 in the supernatants of mTECs. (B-C) Immunoblot assay to assess the expression of the apoptosis-related proteins BCL-2 and cleaved-caspase3. (D-E) Annexin V/PI dual staining for cell apoptosis measurements (n ≥ 3). **(F-K)** LNA anti-miR-21 (100 nM, 24 h) was applied to myotubes to eliminate miR-21 expression before hypoxia and reoxygenation preconditioning; the control group was treated with anti-Scramble. (F) qPCR was used to measure the level of miR-21 after treatment with LNA anti-miR-21 (100 nM, 24 h) or with anti-scramble. LNA anti-miR-21 efficiently knocked down the miR-21 level in myotubes (n = 4). (G) Supernatant concentrations of IL-6 were measured using an enzyme-linked immunosorbent assay (n = 4). (H-I) Immunoblot analysis of the expression of apoptosis-related proteins (n = 3). (J-K) Annexin V/PI dual staining for cell apoptosis measurements. Representative density plots of cell apoptosis after staining are shown. The proportion of apoptotic cells is presented for both early (Annexin V+/PI −) and late (Annexin V+/PI+) apoptotic cells in comparison with the proportion of live cells (Annexin V−/PI−) (n ≥ 3). *p < 0.05, and **p < 0.01. The data are presented as the mean ± SEM.

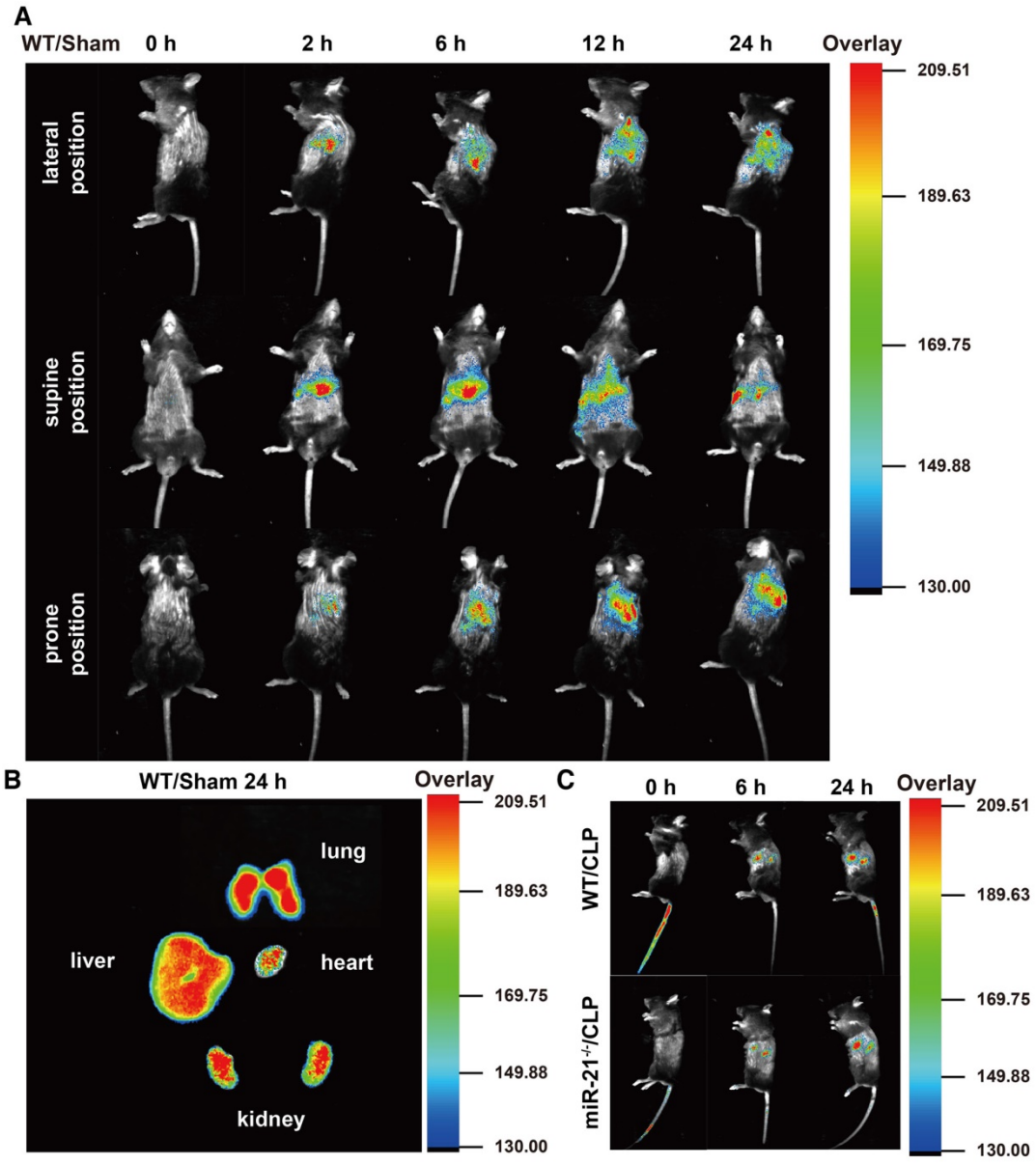

Figure 8. The biodistribution of exogenous exosomes in mice with or without CLP challenge. Exosomes (30 μg) from hypoxia-pretreated myotubes were infused into mice immediately after CLP execution. The control group were infused with an equivalent volume of PBS. **(A)** *In vivo* fluorescence images of WT mice in the sham group at 0, 2, 6, 12, and 24 h post injection with DiR-myotubes in the lateral, supine and prone position (n = 3). **(B)** Ex vivo signals in the dissected organs at 24 h postinjection (n = 3). **(C)** *In vivo* fluorescence images in the lateral position of WT mice and miR-21$^{-/-}$ mice both in the CLP group at 0, 6, and 24 h post injection of DiR-myotubes (n = 3).

Discussion

In the present study, we demonstrated that limb rIPC protected mouse kidneys from septic AKI. This protective effect was associated with elevation of miR-21 in mouse serum exosomes and inhibition of miR-21 target signaling in the kidney. The renoprotection was abolished by systemic deletion of miR-21 or inhibition of HIF-1α expression in skeletal muscles. Additionally, infusion of exogenous exosomes efficiently protected miR-21$^{-/-}$ and WT mice from sepsis-induced organ injury. These findings indicate that, via shuttling of exosomal miR-21, limb rIPC might play a crucial role in preserving renal function against septic AKI and shows potential therapeutic value.

Our results, combined with those of other studies, reveal that more emphasis should be placed on a solution addressing the release of inflammatory cytokines and the loss of tubular epithelial cells in response to sepsis to prevent sepsis-induced AKI [25-27]. MiR-21, a well-established modulator [21,28, 29], has several validated targets, including PDCD-4 and PTEN, both of which act as efficient pro-apoptotic regulators [30-33]. PDCD-4 is also involved in promoting inflammation. Higher miR-21 expression results in lower PDCD-4 expression after LPS

administration, and this effect is due to abrogation of NF-κB activity [34]. In agreement with these previous studies, we found that the abundant expression of miR-21 in kidneys, which was a response to limb rIPC, suppressed PDCD-4 and PTEN expression, decreased NF-kB activity, downregulated cleaved caspase3 expression, and consequently reduced inflammation and apoptosis, attenuating renal injury induced by sepsis. Limb rIPC was shown to exert renal protective effects by upregulating miR-21 expression because inhibition or deletion of miR-21 abolished the renoprotection in sepsis, suggesting that miR-21 may be essential for organ protection. However, direct administration of anti-miR-21 or a miR-21 mimic appears to be limited in application due to their systemic and disease-specific effects [35]. Therefore, a search for an appropriate means of application is necessary. In the present study, we demonstrated that high systemic expression of miR-21, possibly derived from skeletal muscles, could be promoted by limb rIPC, and this beneficial stimulus remained efficient for 24 h.

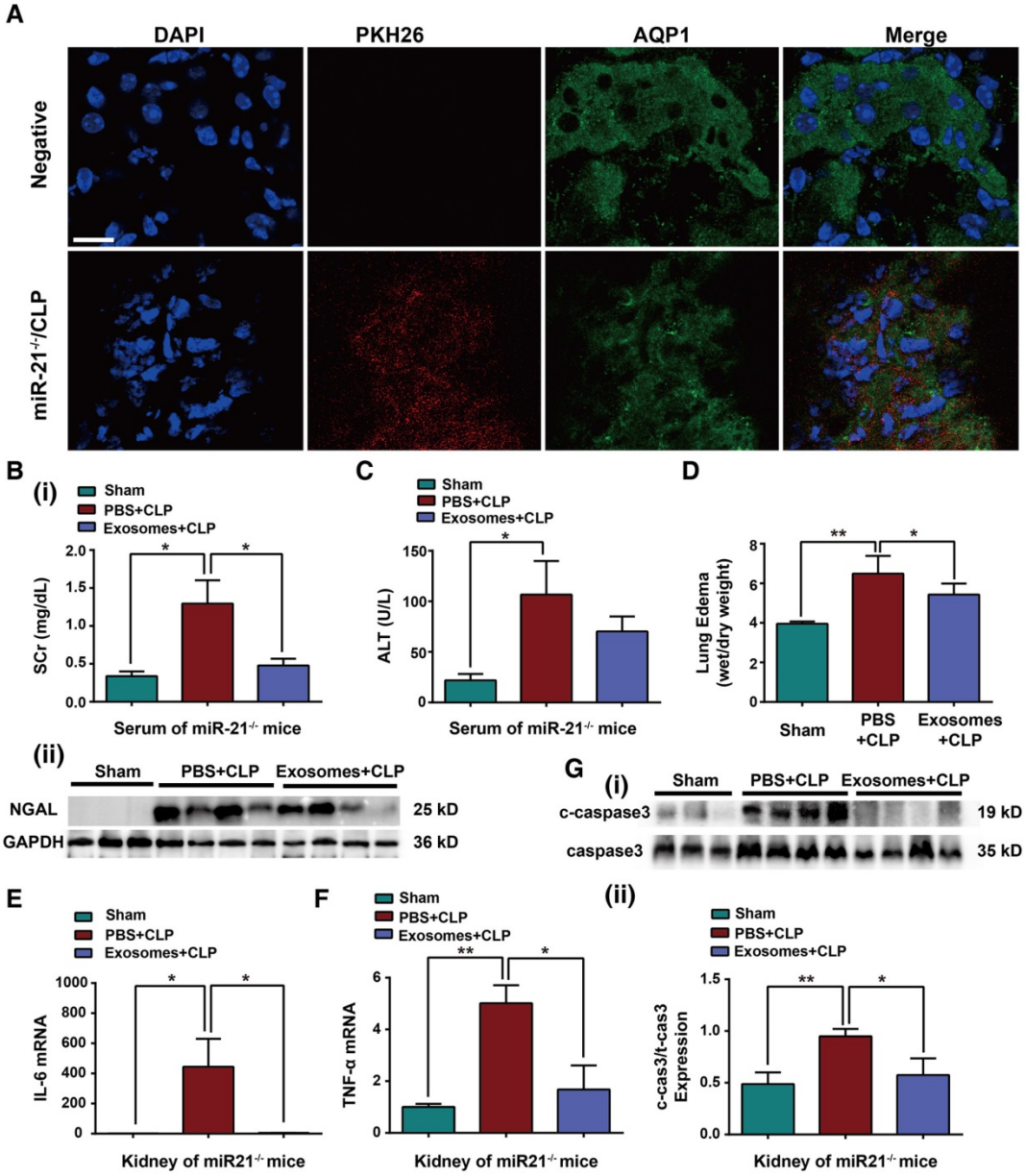

Figure 9. Exosomal miR-21 rescues the organ dysfunction of miR-21$^{-/-}$ mice with CLP injury. Exosomes (30 μg) from hypoxia-pretreated myotubes were infused into miR-21$^{-/-}$ mice immediately after CLP. **(A)** Confocal microscopy analysis of exosomes labeled with PKH26 dye (red) in mouse renal tubular epithelium (AQP1, green) of miR-21$^{-/-}$ mice. The nuclei of the epithelial cells were stained with DAPI. The upper panel shows the negative control cells without exosome injection. (Scale bar, 40 μm). **(B)** Evaluation of serum creatinine and NGAL protein expression was performed in CLP-challenged miR-21$^{-/-}$ mice after exosome infusion (n ≥ 3). **(C)** Serum alanine transaminase (ALT) was also measured among different groups of miR-21$^{-/-}$ mice (n = 4). **(D)** The degree of lung edema was analyzed according to the tissue wet/dry weight ratio in miR-21$^{-/-}$ mice (n = 4). **(E-F)** IL-6 and TNF-α mRNA expression in kidneys after exosome infusion and CLP in miR21$^{-/-}$ mice determined by qPCR (n = 4). **(G)** Immunoblot analysis of cleaved caspase-3 (c-caspase3) in kidneys after exosome infusion and CLP in miR21$^{-/-}$ mice (n ≥ 3). *p < 0.05, and **p < 0.01. The data are presented as the mean ± SEM.

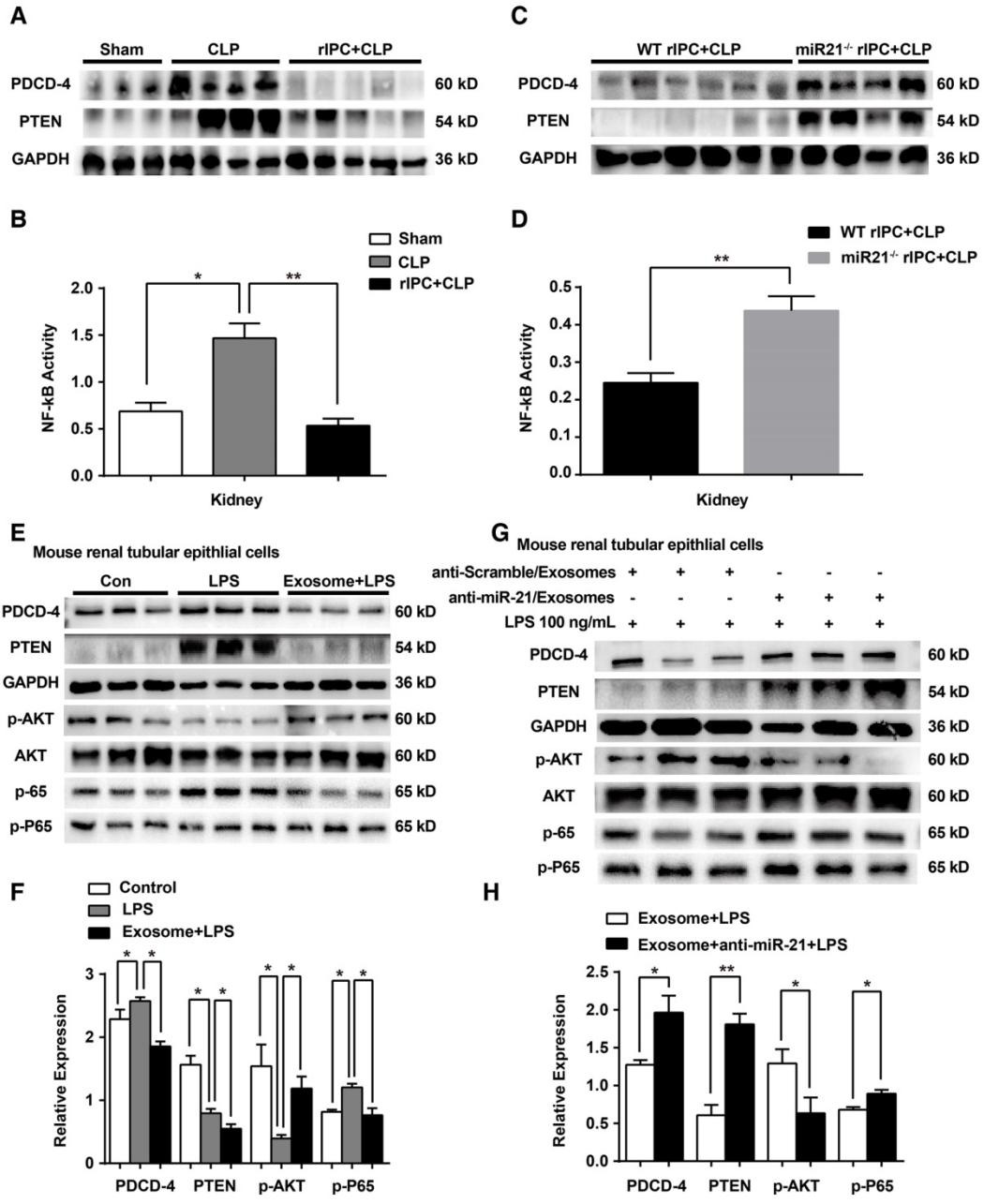

Figure 10. miR-21 inhibits the PDCD4/NF-κB and PTEN signaling pathways in the kidney. (A, C) Immunoblot analysis showing that limb rIPC suppressed PDCD-4 and PTEN expression in the kidneys induced by CLP challenge (n ≥ 3). MiR-21 knockout significantly upregulated PDCD-4 and PTEN expression, even after limb rIPC, compared with the WT littermates that received CLP 24 h after limb rIPC (n ≥ 3). **(B, D)** Assessment of NF-κB activity in the kidneys; limb rIPC inhibited NF-κB activity (n ≥ 3). NF-κB activity was increased in miR-21 knockout mice compared with that in WT littermates (n ≥ 4). **(E, G)** Immunoblot analysis of mTECs; LPS administration upregulated the PDCD-4, PTEN and phospho-P65 (p-P65) levels in mTECs and downregulated phospho-AKT (p-AKT) levels. Preadministration of myotube-derived exosomes reversed the levels of the above proteins in mTECs (n ≥ 3). **(F, H)** Myotube-derived exosomes were pretransferred with LNA anti-miR-21, and the control cells were pretransferred with an anti-Scramble construct. Exosomes with miR-21 knockdown were incapable of reducing the PDCD-4, PTEN and phospho-P65 levels induced by LPS in mTECs, while AKT phosphorylation was suppressed (n ≥ 3). *p < 0.05, and **p < 0.01. The data are presented as the mean ± SEM.

IPC that is applied to multiple parenchymal organs confers strong protective effects in local tissue against subsequent injury [36,37]. In a previous study examining IPC in the kidney, the short-lived episodes of renal ischemia was demonstrated to be an efficient stimulus to evoke upregulation of local miR-21 expression, which serves as a protective effector against sepsis injury [20]. However, the obvious hazards of directly applying IPC to parenchymal organs restrict its application. Limb rIPC induced in femoral arteries is a potentially safer and more promising tool to benefit septic organs [12,38,39]. Limb rIPC has been applied in some clinical studies and shows a potential advantage in renal protection among AKI patients [8]. A brief episode of ischemia and reperfusion in the bilateral iliac vessels of patients

lessens the incidence of postoperative renal injury [40]. Here, we first show the protective efficacy of limb rIPC against septic AKI. In our mouse models, the increased miR-21 produced was available in mice with IPC of the limbs. We also measured the level of miR-21 at different time points following exposure to limb rIPC. A high miR-21 level was observed in skeletal muscles and multiple organs at 2 h post-rIPC but dropped slightly at 6 h, and stable miR-21 expression was maintained for 24 h post-rIPC. These increases in miR-21 expression may be achieved by accurate blocking of the lower extremity arteries in mice [41-43].

HIF-1α, an important transcription factor, has been well-documented as an oxygen-sensitive mediator to orchestrate protective process in response to hypoxia [44-46]. Many studies have demonstrated that HIF-1α is an efficient regulator of early and delayed IPC against subsequent ischemia injury [47,48]. In addition, a number of studies have investigated the role of HIF-1α in regulating miRNA function through miRNA translocation to the nucleus and binding with hypoxia-responsive element sequences in target promoters [49-51]. According to our previous study, a potential hypoxia-responsive element (HRE) binding site is present in the promoter region of miR-21, which is positively modulated by increases in HIF-1α expression [20]. Therefore, HIF-1α, the recognized factor present under ischemic conditions [52], may explain the effects of limb rIPC and subsequent miR-21 production against CLP challenge observed in the present study. We also observed that knockdown of HIF-1α in skeletal muscle inhibited miR-21 expression post-rIPC and abrogated its protective effect against CLP, and these data further suggested the critical importance of miR-21 in protecting the mice from septic AKI, depending on the accumulation and stabilization of HIF-1α induced by limb rIPC.

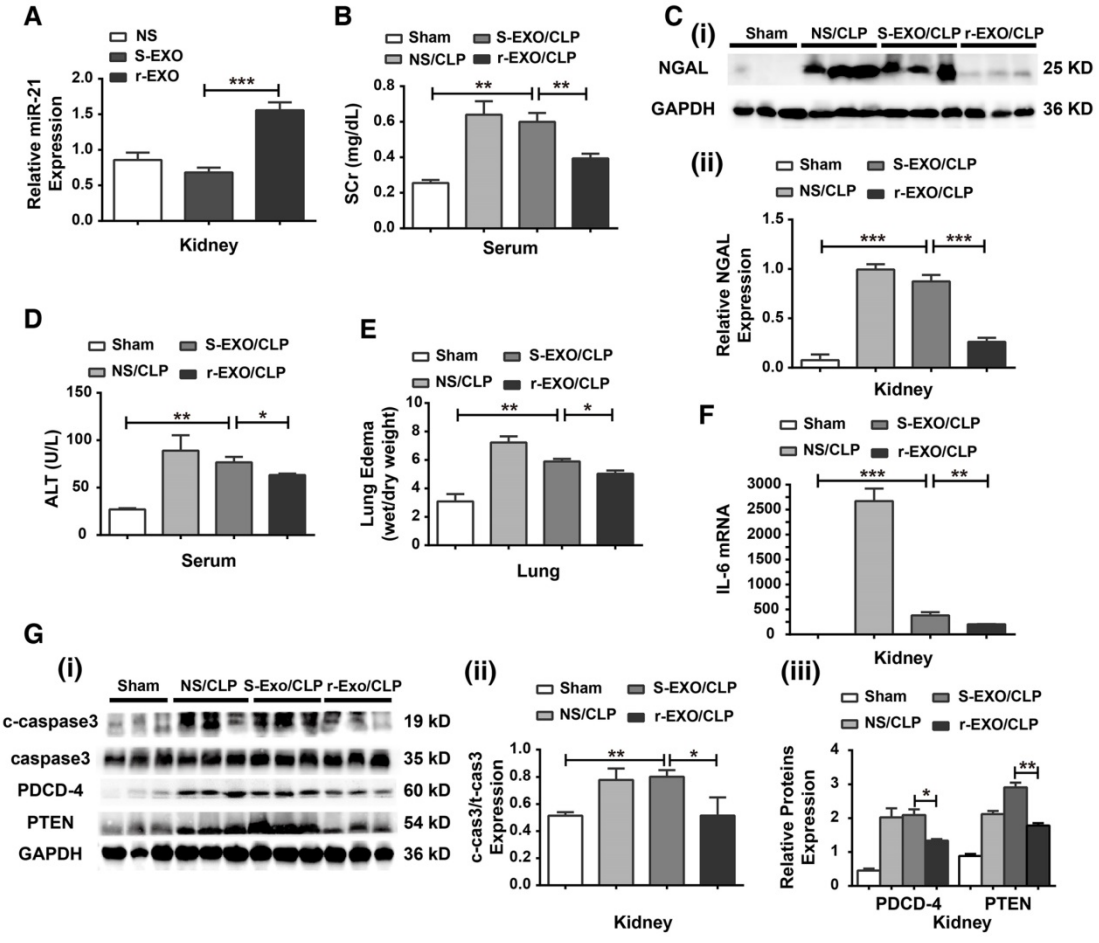

Figure 11. Exosomes derived from rIPC-treated mice protected mice from CLP injury. Exosomes (200 μg in 100 μL of NS) extracted from the serum of rIPC-treated mice, sham-treated mice or normal saline (NS)-treated mice were infused into recipient mice immediately after CLP challenge. Mice were divided into the following groups: a sham group, NS/CLP group, sham-exosome-treated group (S-EXO/CLP) and rIPC-exosome-treated group (r-EXO/CLP). **(A)** miR-21 levels were evaluated among mice infused with NS, S-EXO or r-EXO without CLP injury. r-EXO infusion significantly upregulated miR-21 expression in the kidneys of mice compared with S-EXO-treated mice (n = 6). **(B)** The serum creatinine and NGAL protein expression was level assessed in various groups (n = 6). **(C-D)** The alanine transaminase (ALT) level and degree of lung edema were also evaluated (n = 6). **(E)** qPCR assay of the IL-6 mRNA expression level in kidneys (n = 6). **(G)** Immunoblot analysis of cleaved caspase-3 (c-caspase3) and signaling proteins related to miR-21 (PDCD-4 and PTEN) in kidneys (n = 6). *p < 0.05, and **p < 0.01. The data are presented as the mean ± SEM.

However, HIF-1α activation was not detected in the kidney or lung, while high miR-21 expression was found at these sites, which suggested a potential carrier that delivers the miRNA into these target organs. Exosomes, which are a type of nanoparticle, function as intercellular shuttles that bud from the host cell membrane and carry information to recipient cells [53-55]. In this study, we demonstrated that exosomes derived from cultured H/R myotubes successfully fused with the membranes of mTECs. Upregulation of miR-21 in myotube-derived exosomes clearly inhibited inflammation and apoptosis in an *in vitro* septic AKI model. Additionally, secreted exosomes can be transferred in biological fluids to interact with remote organs [56]. As shown in our study, miR-21 expression in exosomes extracted from the serum of mice with limb rIPC and humans with noninvasive rIPC was significantly upregulated and sustained for 24 h, which met the requirements of remote organ protection in the mouse CLP model, and HIF-1α knockdown inhibited miR-21 expression in circulating exosomes. Therefore, exosomes might be reliable cargo carriers for the effectors of limb rIPC. Additionally, infusion of exosomes derived from H/R myotubes into CLP model mice was performed, and replenishment of the exogenous exosomes, with abundant miR-21 expression, restored the renal function of miR-21$^{-/-}$ mice. Rescue experiments with stem cell-derived exosomes have also been validated based on the improvement in spatial learning of mice suffering from Alzheimer's disease (AD) [57]. The previous data combined with our results suggest that exosome infusion is a promising approach for treatment and prevention of septic AKI as well as for other diseases.

This study has some limitations. Although limb rIPC efficiently induced higher expression of myogenin protein, a muscle differentiation marker [62], in mouse serum exosomes, whether exosomal miR-21 in circulation is directly produced by skeletal muscles remains unclear. Meanwhile, whether any additional effectors or miRNAs are involved in the observed renal protection has not been elaborated and requires further investigation.

In conclusion, our present data indicate that the systemic upregulation of miR-21 induced by limb rIPC confers anti-inflammatory and anti-apoptotic effects against septic AKI. This enriched miRNA is likely transferred via exosomes to benefit distant organs. Limb rIPC might serve as a possible therapeutic strategy and potentially lead to progress in translation of rIPC from the bench to the bedside.

Methods

Animals

Male miR-21$^{-/-}$ (C57BL/6) mice and their WT littermates were generated by Shanghai Model Organisms Center, Inc. Before surgery, mice aged 8-10 weeks were bred in our animal facilities with free access to sterile water and clean food. Mice weighing 20-25 g were used in our experiments. The mice were randomized into the following groups: a sham group, rIPC group, CLP group and rIPC+CLP group and an NS-injection (intraperitoneal injection) group, LPS-injection group and rIPC+LPS group (n = 4-6 in each group). The mice in all groups were anaesthetized by intraperitoneal (IP) injection of 1% (50 mg/kg) sodium pentobarbital before surgery. The experiments were approved by the Institutional Animal Care and Use Committee of Fudan University.

Human sample collection

This study was conducted with the permission of the ethics committee of Fudan University. Written consent was obtained from each healthy participant, who had a negative medical history for any cardio-cerebrovascular disease and who was informed of the procedure and potential risk. rIPC was performed with four cycles of a 5-min inflation to 200 mmHg and a 5-min deflation with a manually operated upper-arm cuff inflator. Ten-milliliter serum separator tubes were used to collect blood samples before rIPC was performed and at 2, 12, and 24 h after rIPC. The samples were centrifuged at 2,500 ×*g* for 10 min for serum extraction, and the serum was stored at -80 °C.

Limb remote ischemic preconditioning

An incision was made in the femoral triangle in mice of all groups, and the bilateral femoral arteries were separated from the femoral artery sheaths and subsequently received 4 cycles of I/R with 5 min of clamping and 5 min of unclamping using microvascular clips. The mice in the sham group and the mice to be challenged with CLP underwent identical surgical procedures, except the sham group did not undergo clamping of the arteries.

Induction of polymicrobial sepsis and endotoxemia in mice

Abdominal sepsis was induced according to a previous procedure [58]. Briefly, the cecum was brought outside the mouse and returned to the abdomen; however, the sham group and rIPC alone group were not subjected to cecal puncture or perforation or the squeezing of a small amount of feces. The endotoxemia mouse model was induced via

intraperitoneal injection of LPS from Escherichia coli 055:B5 (Sigma, St. Louis, MO) at a dose of 20 mg/kg. Intraperitoneal injection of saline served as the control.

Survival rate analysis

The mice were divided into three groups: a sham group, CLP group and rIPC+CLP group (n = 10 in each group). After CLP execution, mice in multiple groups were observed for an additional time (7 days) to assess the survival rate. The time of death for these animals was observed and recorded by one researcher who was blinded to the assignment.

Cell culture and H/R

Mouse renal tubular epithelial cells (mTECs) were a gift from the Urology Department of Zhongshan Hospital affiliated with Fudan University. The cells were cultured in DMEM with 10% fetal bovine serum (FBS) in a humidified incubator with 5% CO_2/95% air. C2C12 cells (American Type Culture Collection, USA) were cultured in DMEM supplemented with 4.5 mg glucose and 10% FBS in a 5% CO_2/95% air incubator at 37 °C. When the cultured C2C12 cells reached 100% confluence, myotubes differentiation was induced by incubating the cells with DMEM and 2% horse serum (HS) for 5 to 7 days. For hypoxia, myotubes were washed with PBS twice, cultured in DMEM without FBS, and transferred to a hypoxia incubator (Thermo scientific, USA), which was equipped with a gas mixture comprising 1% O_2 and 5% CO_2, balanced with N_2). The hypoxia and reoxygenation (H/R) protocol consisted of 6 or 24 h of hypoxia followed by 4 h of reoxygenation. Before this step, partial myotubes were transfected with 100 nM LNA anti-miR-21 using Lipofectamine 3000 for 48 h to eliminate miR-21 expression, and cells transfected with anti-Scramble were set as the control.

A cellular septic AKI model was generated with LPS. mTECs were treated with 100 ng/mL LPS for 24 h, and the cells in the control group were treated with cell culture medium (vehicle).

Isolation and injection of exosomes

Exosomes were isolated from mouse serum, human serum samples and supernatants of myotubes as previously described with some modifications [59]. Differentiated C2C12 cells (myotubes) were grown in 10-cm dishes in DMEM without FBS under H/R or normoxia treatment. Then, the medium was collected, centrifuged at 3,000 ×*g* for 15 min and filtered through a 0.2-mm pore filter (Millipore, USA). The collected supernatant was then ultracentrifuged at 100,000 ×*g* for 6 h at 4 °C. Afterwards, PBS or a specific buffer was used to dilute the extractions. Serum samples were mixed in 11 mL of PBS and filtered through a 0.2-mm pore filter. Then, the mixture was ultracentrifuged at 100,000 ×*g* overnight at 4 °C. Afterwards, the supernatants were discarded, and the pellets were diluted in PBS or other buffers for further identification or analysis. The protein concentrations of the isolated exosomes were evaluated with bicinchoninic acid assay (BCA) protein assays. Mice were treated with the cell-derived exosomes (30 μg) or autologous murine serum-derived exosomes (200 μg) through the lateral caudal vein immediately after the CLP challenge. The control group was injected with PBS.

Serum creatinine and lung edema

A total of 0.7-1.0 mL of blood was collected from the jugular veins of mice. The serum was gathered after centrifugation at 3,000 ×*g* for 25 min. The serum creatinine concentrations were determined using a creatinine assay kit (Bio Assay Systems, USA). The left lung was then air-dried at 60 °C for 72 h and reweighed. The wet weight to dry weight ratio was determined to indicate the formation of lung edema.

Alanine transaminase assays

The serum alanine transaminase (ALT) level in each sample was evaluated using an Alanine Transaminase Assay Kit (BioAssay Systems, USA) in accordance with the manufacturer's instructions.

Histology

Tissues were fixed in 4% formaldehyde phosphate buffer overnight and then dehydrated, followed by paraffin embedding; 4-μm sections were prepared and stained with hematoxylin and eosin (HE). The tissue injury scores were quantified in a blinded fashion. Renal tissue injury was determined as follows: tubular dilatation, vacuolization, tubular cell necrosis, loss of brush border, interstitial edema and inflammatory cell infiltration.

ELISAs

The IL-6 and TNF-α levels in the serum and kidneys were measured with commercial ELISA kits (R&D Systems Inc., USA), and NF-κB activity in renal tissues was measured using a Trans AM NF-κB p65 kit (Active Motif, CA, USA).

Immunohistochemical staining

Immunohistochemical staining was performed on 4-μm paraffinized sections. The samples were dewaxed, dehydrated, washed in PBS, incubated with 3% H_2O_2 for 20 min to quench endogenous peroxidase activity and incubated with normal goat serum (1:20) for 30 min. Afterward, the samples were treated with anti-MPO antibody (rabbit polyclonal, 1:500; Service-bio, China) at 4 °C overnight. The sections were then

incubated with a horseradish peroxidase-conjugated secondary antibody (anti-rabbit IgG; Servicebio, China) for 2 h at room temperature. After being washed three times with PBS, the sections were stained with 3,30-diaminobenzidine (DAKO, China) and subsequently stained with hematoxylin. Then, the number of positive cells was evaluated under a light microscope. Ten areas were randomly selected. The sections were scored according to the number of MPO-positive cells per high power field (HP) in a blinded manner.

TUNEL assay

To determine the level of cell apoptosis in the kidneys, TUNEL assays were performed using a commercial kit (FragEL DNA Fragmentation Detection Kit; Millipore, USA) according to the manufacturer's protocol. The number of staining-positive cells in ten random areas was determined using a light microscope. The TUNEL-positive cells are expressed as the number of staining-positive cells per high power field (HP).

Western blotting

Western blotting was performed as described in a previous study [60]. Antibodies targeting the following proteins were used: CD63 and PDCD4 (Novus, CO, USA); BCL-2, total caspase3, cleaved-caspase3, p-AKT, AKT, PTEN, p-P65 and P65 (Cell Signaling Technology, MA, USA); HIF-1α (Bioworld, MN, USA); NGAL (R&D systems, USA); myogenin (R&D systems, USA) and GAPDH (Santa Cruz Biotechnology, TX, USA).

qPCR assay

TRIzol (Sigma, USA) was introduced to extract total RNA from kidneys, lungs, serum exosomes, mTECs, differentiated C2C12 cells (myotubes) and cell supernatant exosomes. The IL-6 mRNA, TNF-α mRNA and miR-21 expression levels were analyzed via real-time PCR as described in a previous study (β-actin and U6 were set as the housekeeping genes, respectively) [61].

Extraction of exosomal proteins and RNA

Pelleted exosomes from serum were resuspended in 500 μL of TRIzol (Sigma, USA) for qPCR analysis or in 200 μL of lysis buffer (Beyotime Biotechnology, China) for protein analysis, while exosomes from the cell supernatants were diluted in 250 μL of TRIzol or 100 μL of lysis buffer [59].

Confocal microscopy

For exosome uptake analysis, exosomes derived from myotubes (1×10^6) treated with H/R were diluted in 100 μL of PBS. Subsequently, the suspension was incubated with 0.2 μL of PKH26 (Sigma, USA) combined with 10 μL of Diluent C for 5 min at 37 °C. Then, 120 μL of 1% BSA was added to stop the reaction, and the mixture was further suspended in 1 mL of PBS. Afterward, 100 μL of Exosome Precipitation Solution from an ExoQuick TC kit was added and incubated with the mixture overnight at 4 °C. Then, a pellet of the mixture was obtained by centrifugation at 1,500 ×*g* for 30 min, and 200 μL of the resuspended pellet was transferred to mTECs that had been grown on coverslips for 12 h in a 5% CO_2/95% air incubator at 37 °C. DAPI was used for nuclear staining. Images were recorded on a Zeiss LSM 700 confocal microscope (Germany). The z-stacks were 0.36 μm.

Flow cytometry

The ratio of apoptotic mTECs was determined by flow cytometric analysis with an Annexin V/PI kit (BD Bioscience, USA) according to the manufacturer's instructions.

Transmission electron microscopy

To examine the morphology of exosomes, electron microscopic analysis was performed. A suspension of the exosome pellet was mixed with an equal volume of 4% paraformaldehyde, placed on a Formvar-carbon-coated electron microscopy grid, incubated with 1% glutaraldehyde for 5 min, and subjected to standard uranyl acetate staining. The sample was washed with PBS and observed using a transmission electron microscope (Hitachi H7500 TEM, Japan). A microBAR was used to evaluate the diameters of the exosomes.

Nanoparticle trafficking analysis

The size distribution and concentration of the extracted exosomes were determined using a nanoparticle tracking system (ZETASIZER Nano Series, UK) by Dynamic Light Scattering (DLS) assay according to a previous study [60]. After isolation, the particles were resuspended in 1 mL of filtered PBS. Filtered PBS was used as the control.

HIF-1α siRNA injection into skeletal muscles

To knock down HIF-1α expression in murine skeletal muscles, HIF-1α siRNA (GenePharma, China) mixed with *in vivo* jetPEI (Polyplus transfection, USA) was delivered to the skeletal muscles at two different sites (the adductor muscle and the gastrocnemius) of the bilateral hind limbs by intramuscular injection. To prepare PEI-siRNA mixtures, according to the manufacturer's protocol, HIF-1α siRNA (10 μg) or a negative control (NC) in 5% glucose was mixed with jetPEI solution to achieve a 100-μL total injection volume. After 2 h, the mice in the different groups

were subjected to brief ischemia and reperfusion.

Fluorescence imaging of DiR exosomes

Isolated exosomes were incubated with 35 μg/mL Lipophilic Tracers-DiR buffer for 30 min at 37 °C according to the manufacturer's protocol (Invitrogen, USA). One percent BSA was added to terminate the reaction. Then, the DiR-exosome mixture was mixed with an identical volume of ExoQuick Exosome Precipitation Solution (System Biosciences, USA) and incubated at 4 °C overnight. Then, to remove the residual dye, the mixture was centrifuged at 14,000 ×*g* for 15 min. DiR exosomes (30 μg) were then resuspended in 200 μL PBS buffer.

DiR exosomes (30 μg) were intravenously injected into mice (n = 3) in different groups. The biodistribution of DiR exosomes was monitored using a HealthCare Stream system (USA) at 0, 2, 6, 12, and 24 h postinjection. Filters allowing excitation at 720 nm and collection of emission at 790 nm were used to obtain ideal images. Identical experimental conditions were used in all mice, which were photographed in lateral, supine and prone positions. Mouse heart, lung, liver and kidneys were dissected for ex vivo evaluation at 24 h postinjection. Grayscale backgrounds and fluorescence images of each sample were overlaid using the HealthCare Stream system software (USA).

miR-21 knockout mice

miR-21 knockout mice were generated in Shanghai Model Organisms Center, Inc. The mouse generation details have been elaborated in previous studies [20].

Knockout mice were identified by RT-PCR with the following primers: forward, 5′-CAGAATTGCCC AGGCTTTTA-3′; and reverse, 5′- AATCCATGAGGC AAGGTGAC -3′.

Statistical analysis

All results are presented as the mean ± S.E.M. Unpaired t-tests and one-way ANOVA were performed using GraphPad Prism version 6.0 software for Mac (GraphPad Software, Inc., USA) to determine p-values. $P<0.05$ was defined as statistically significant. The normal distribution of data was assessed by the Kolmogorov-Smirnov test.

Supplementary Material

Supplementary figures and tables.
http://www.thno.org/v09p0405s1.pdf

Acknowledgements

This work was supported by the National Natural Science Foundation of China (81670614 and 81430015 to Xiaoqiang Ding), the Science and Technology Commission of Shanghai Municipality (14DZ2260200, the project of Shanghai Key Laboratory of Kidney and Blood Purification), National Natural Science Foundation of China (81471890 to Ping Jia).

Author Contributions

Tianyi Pan, Ping Jia and Xiaoqiang Ding designed the study; Tianyi Pan, Nan Chen and Yiran Liang carried out experiments; Tianyi Pan, Ping Jia and Yi Fang analyzed the data; Tianyi Pan, Ping Jia and Man Guo made the figures; Tianyi Pan, Ping Jia and Xiaoqiang Ding drafted and revised the paper; all authors approved the final version of the manuscript.

Competing Interests

The authors have declared that no competing interest exists.

References

1. Abraham E. New definitions for sepsis and septic shock: continuing evolution but with much still to be done. JAMA. 2016; 8: 757-759.
2. Prowle JR. Sepsis-associated AKI. Clin J Am Soc Nephrol. 2018; 13: 339-342.
3. Singbartl K, Kellum JA. AKI in the ICU: definition, epidemiology, risk stratification, and outcomes. Kidney Int. 2012; 9: 819-25.
4. Singer M, De Santis V, Vitale D, Jeffcoate W. Multiorgan failure is an adaptive, endocrine-mediated, metabolic response to overwhelming systemic inflammation. Lancet. 2004; 9433: 545-548.
5. Wu L, Gokden N, Mayeux PR. Evidence for the role of reactive nitrogen species in polymicrobial sepsis-induced renal peritubular capillary dysfunction and tubular injury. J Am Soc Nephrol. 2007; 6: 1807-1815.
6. Birnbaum Y, Hale SL, Kloner RA. Ischemic preconditioning at a distance: reduction of myocardial infarct size by partial reduction of blood supply combined with rapid stimulation of the gastrocnemius muscle in the rabbit. Circulation. 1997; 96: 1641–1646.
7. Chen K, Xu Z, Liu Y, Wang Z, Li Y, Zeng C. Irisin protects mitochondria function during pulmonary ischemia/reperfusion injury. Sci Transl Med. 2017; 9: 418.
8. Zarbock A, Schmidt C, Van Aken H, Wempe C, Martens S, Meersch M. Effect of remote ischemic preconditioning on kidney injury among high-risk patients undergoing cardiac surgery: a randomized clinical trial. JAMA. 2015; 21: 2133-41.
9. Davidson SM, Selvaraj P, He D, Boi-Doku C, Yellon RL, Yellon DM. Remote ischemic preconditioning involves signaling through the SDF-1alpha/CXCR4 signaling axis. Basic Res Cardiol. 2013; 108: 377.
10. Liu T, Fang Y, Liu S, Yu X, Liang M, Ding X. Limb ischemic preconditioning protects against contrast-induced acute kidney injury in rats via phosphorylation of GSK-3β. Free RadicBiol Med. 2015; 81: 170-82.
11. Lim SY, Yellon DM, Hausenloy DJ. The neural and humoral pathways in remote limb ischemic preconditioning. Basic Res Cardiol. 2010; 105: 651–655.
12. Cai Z, Luo W, Zhan H, Semenza GL. Hypoxia-inducible factor 1 is required for remote ischemic preconditioning of the heart. Proc Natl Acad Sci. 2013; 43: 17462-7.
13. Konstantinov IE, Arab S, Li J, Coles JG, Boscarino C, Redington AN. The remote ischemic preconditioning stimulus modifies gene expression in mouse myocardium. J ThoracCardiovasc Surg. 2005; 5: 1326-32.
14. Li J1, Rohailla S, Gelber N, Rutka J, Sabah N, Redington AN. MicroRNA-144 is a circulating effector of remote ischemic preconditioning. Basic Res Cardiol. 2014; 109: 423.
15. Krol J, Loedige I, Filipowicz W. The widespread regulation of microRNA biogenesis, function and decay. Nat Rev Genet. 2010; 11: 597–610.
16. Mitchell PS, Parkin RK, Kroh EM, Fritz BR, Wyman SK, Tewari M et al. Circulating microRNAs as stable blood-based markers for cancer detection. Proc Natl Acad Sci. 2008; 105: 10513-8.
17. Xiao B, Wang Y, Li W, Baker M, Guo J, He YW. Plasma microRNA signature as a non-invasive biomarker for acute graft-versus-host disease. Blood. 2013; 122: 3365.
18. Yamaguchi T, Izumi Y, Nakamura Y, Yamazaki T, Shiota M, Iwao H. Repeated remote ischemic conditioning attenuates left ventricular remodeling via exosome-mediated intercellular communication on chronic heart failure after myocardial infarction. Int J Cardiol. 2015; 178: 239-46.
19. Slagsvold KH, Rognmo O, Hoydal M, Wisloff U, Wahba A. Remote ischemic preconditioning preserves mitochondrial function and influences myocardial

microRNA expression in atrial myocardium during coronary bypass surgery. Circ Res. 2014; 114: 851–859.
20. Jia P, Wu X, Dai Y, Teng J, Liang M, Ding X. MicroRNA-21 Is Required for Local and Remote Ischemic Preconditioning in Multiple Organ Protection Against Sepsis. Crit Care Med. 2017; 45: 703-710.
21. Sayed D, He M, Hong C, Gao S, Rane S, Abdellatif M. MicroRNA-21 is a downstream effector of AKT that mediates its anti-apoptotic effects via suppression of Fas ligand. J Biol Chem. 2010; 285: 20281-90.
22. Xu X, Kriegel AJ, Liu Y, Usa K, Ding X, Liang M, et al. Delayed ischemic preconditioning contributes to renal protection by up-regulation of miR-21. Kidney Int. 2012; 82: 1167-75.
23. Lerolle N, Nochy D, Guérot E, Bruneval P, Fagon JY, Hill G. Histopathology of septic shock induced acute kidney injury: apoptosis and leukocytic infiltration. Intensive Care Med. 2010; 36: 471-8.
24. Liu Y, Nie H, Zhang K, Ma D, Yang G, Yang S. A feedback regulatory loop between HIF-1 α and miR-21 in response to hypoxia in cardiomyotubes. FEBS Lett. 2014; 588: 3137-46.
25. Langenberg C, Gobe G, Hood S, May CN, Bellomo R. Renal histopathology during experimental septic acute kidney injury and recovery. Crit Care Med. 2014; 42: 58-67.
26. Poukkanen M, Wilkman E, Vaara ST, Pettilä V, Kuitunen A, Karlsson S, et al. Hemodynamic variables and progression of acute kidney injury in critically ill patients with severe sepsis: data from the prospective observational FINNAKI study. Crit Care. 2013; 17: 295.
27. Gomez H, Ince C, De Backer D, Pickkers P, Payen D, Kellum JA et al. A unified theory of sepsis-induced acute kidney injury: inflammation, microcirculatory dysfunction, bioenergetics, and the tubular cell adaptation to injury. Shock. 2014; 41: 3-11.
28. Maegdefessel L, Azuma J, Toh R, Deng A, Merk DR, Tsao PS et al. MicroRNA-21 blocks abdominal aortic aneurysm development and nicotine-augmented expansion. Sci Transl Med. 2012; 4: 122-22.
29. Caescu CI, Guo X, Tesfa L, Bhagat TD, Verma A, Stanley ER. Colony stimulating factor-1 receptor signaling networks inhibit mouse macrophage inflammatory responses by induction of microRNA-21. Blood. 2015; 125: 1-13.
30. Frankel LB1, Christoffersen NR, Jacobsen A, Lindow M, Krogh A, Lund AH. Programmed cell death 4 (PDCD4) is an important functional target of the microRNA miR-21 in breast cancer cells. J Biol Chem. 2008; 283: 1026-33.
31. Wu Y, Song Y, Xiong Y, Wang X, Xu K, Zhou L. MicroRNA-21 (Mir-21) Promotes Cell Growth and Invasion by Repressing Tumor Suppressor PTEN in Colorectal Cancer. Cell Physiol Biochem. 2017; 43: 945-958.
32. Wang S, Wang J, Zhang Z, Miao H. Decreased miR-128 and increased miR-21 synergistically cause podocyte injury in sepsis. J Nephrol. 2017; 30: 543-550.
33. Xiao J, Pan Y, Li XH, Yang XY, Feng YL, Yu XY, et al. Cardiac progenitor cell-derived exosomes prevent cardiomyotubes apoptosis through exosomal miR-21 by targeting PDCD4. Cell Death Dis. 2016; 23: e2277.
34. Sheedy FJ, Palsson-McDermott E, Hennessy EJ, Martin C, O'Leary JJ, J O'Neill LA, et al. Negative regulation of TLR4 via targeting of the proinflammatory tumor suppressor PDCD4 by the microRNA miR-21. Nat Immunol. 2010; 11: 141-7.
35. Xu X, Kriegel AJ, Jiao X, Liu H, Liang M, Ding X. miR-21 in ischemia/reperfusion injury: a double-edged sword? Physiol Genomics. 2014; 46: 789-97.
36. Joo JD, Kim M, D'Agati VD, Lee HT. Ischemic preconditioning provides both acute and delayed protection against renal ischemia and reperfusion injury in mice. J Am Soc Nephrol. 2006; 17: 3115-23.
37. Davies WR1, Brown AJ, Watson W, McCormick LM, Hoole SP. Remote ischemic preconditioning improves outcome at 6 years after elective percutaneous coronary intervention: the CRISP stent trial long-term follow-up. Circ Cardiovasc Interv. 2013; 6: 246-51.
38. Li C, Xu M, Wu Y, Li YS, Huang WQ, Liu KX. Limb remote ischemic preconditioning attenuates lung injury after pulmonary resection under propofol-remifentanil anesthesia: a randomized controlled study. Anesthesiology. 2014; 121: 249-59.
39. Jensen HA, Loukogeorgakis S, Yannopoulos F, Rimpiläinen E, Petzold A, Juvonen T, et al. Remote ischemic preconditioning protects the brain against injury after hypothermic circulatory arrest. Circulation. 2011; 123: 714-21.
40. Ali ZA, Callaghan CJ, Lim E, Ali AA, Nouraei SA, Gaunt ME, et al. Remote ischemic preconditioning reduces myocardial and renal injury after elective abdominal aortic aneurysm repair: a randomized controlled trial. Circulation. 2007; 116: 98-105.
41. Lawan A, Min K, Zhang L, Canfran-Duque A, 3Jurczak MJ, Bennett AM, et al. Skeletal Muscle-Specific Deletion of MKP-1 Reveals a p38 MAPK/JNK/Akt Signaling Node That Regulates Obesity-Induced Insulin Resistance. Diabetes. 2018; 67: 624-635.
42. Wiegand C, Heusser P, Klinger C, Cysarz D, Büssing A, Savelsbergh A, et al. Stress-associated changes in salivary microRNAs can be detected in response to the Trier Social Stress Test: An exploratory study. Sci Rep. 2018; 8: 7112.
43. Kharbanda RK, Mortensen UM, White PA, Kristiansen SB, Schmidt MR, MacAllister R, et al. Transient limb ischemia induces remote ischemic preconditioning in vivo. Circulation. 2002; 106: 2881-3.
44. Semenza GL. HIF-1: mediator of physiological and pathophysiological responses to hypoxia. J Appl Physiol. 2000; 88: 1474-80.
45. Loor G, Schumacker PT. Role of hypoxia-inducible factor in cell survival during myocardial ischemia-reperfusion. Cell Death Differ. 2008;15: 686-90.
46. Tekin D, Dursun AD, Xi L. Hypoxia inducible factor 1 (HIF-1) and cardioprotection. Acta Pharmacol Sin. 2010; 31: 1085-94.
47. Semenza GL. Hypoxia-inducible factor 1: regulator of mitochondrial metabolism and mediator of ischemic preconditioning. Biochim Biophys Acta. 2011;1813: 1263-8.
48. Hausenloy DJ, Yellon DM. The second window of preconditioning (SWOP) where are we now? Cardiovasc Drugs Ther. 2010; 24: 235-54.
49. Rane S, He M, Sayed D, Vashistha H, Malhotra A, Abdellatif M, et al. Downregulation of miR-199a derepresses hypoxia-inducible factor-1alpha and Sirtuin 1 and recapitulates hypoxia preconditioning in cardiac myotubes. Circ Res. 2009; 104: 879-86.
50. Ghosh G, Subramanian IV, Adhikari N, Zhang X, Joshi HP, Ramakrishnan S, et al. Hypoxia-induced microRNA-424 expression in human endothelial cells regulates HIF-α isoforms and promotes angiogenesis. J Clin Invest. 2010; 120: 4141-54.
51. Cha ST, Chen PS, Johansson G, Chu CY, Wang MY, Kuo ML, et al. MicroRNA-519c suppresses hypoxia-inducible factor-1alpha expression and tumor angiogenesis. Cancer Res. 2010;70: 2675-85.
52. Bernhardt WM, Câmpean V, Kany S, Jürgensen JS, Weidemann A, Eckardt KU et al. Preconditional activation of hypoxia-inducible factors ameliorates ischemic acute renal failure. J Am Soc Nephrol. 2006; 17: 1970–1978.
53. Barile L, Vassalli G. Exosomes: Therapy delivery tools and biomarkers of diseases. Pharmacol Ther. 2017; 174: 63-78.
54. Cheng X, Zhang G, Zhang L, Hu Y, Zhang K, Zhao J, et al. Mesenchymal stem cells deliver exogenous miR-21 via exosomes to inhibit nucleus pulposus cell apoptosis and reduce intervertebral disc degeneration. J Cell Mol Med. 2018; 22: 261-276.
55. Au Yeung CL, Co NN, Tsuruga T, Yeung TL, Kwan SY, Mok SC, et al. Exosomal transfer of stroma-derived miR21 confers paclitaxel resistance in ovarian cancer cells through targeting APAF1. Nat Commun. 2016; 7: 11-150.
56. Karimi N, Cvjetkovic A, Jang SC, Crescitelli R, HosseinpourFeizi M, Lässer C, et al. Detailed analysis of the plasma extracellular vesicle proteome after separation from lipoproteins. Cell Mol Life Sci. 2018.
57. Cui GH, Wu J, Mou FF, Xie WH, Wang FB, Wang QL, et al. Exosomes derived from hypoxia-preconditioned mesenchymal stromal cells ameliorate cognitive decline by rescuing synaptic dysfunction and regulating inflammatory responses in APP/PS1 mice. FASEB J. 2018; 32: 654-668.
58. Chousterman BG, Boissonnas A, Poupel L, Baudesson de Chanville C, Payen D, Combadière C, et al. Ly6C high Monocytes Protect against Kidney Damage during Sepsis via a CX3CR1-Dependent Adhesion Mechanism. J Am Soc Nephrol. 2016; 27: 792-803.
59. Li L, Li C, Wang S, Wang Z, Jiang J, Zhu G. Exosomes Derived from Hypoxic Oral Squamous Cell Carcinoma Cells Deliver miR-21 to Normoxic Cells to Elicit a Prometastatic Phenotype. Cancer Res. 2016; 76: 1770-80.
60. Melo SA, Luecke LB, Kahlert C, Fernandez AF, Gammon ST, Kalluri R. Glypican-1 identifies cancer exosomes and detects early pancreatic cancer. Nature. 2015; 523: 177-82.
61. Huang W, Lan X, Li X, Wang D, Sun Y, Yu K. Long non-coding RNA PVT1 promote LPS-induced septic acute kidney injury by regulating TNF α and JNK/NF-κB pathways in HK-2 cells. Int Immunopharmacol. 2017; 47: 134-140.
62. Cammas A, Sanchez BJ, Lian XJ, Dormoy-Raclet V, van der Giessen K, Gallouzi IE, et al. Destabilization of nucleophosmin mRNA by the HuR/KSRP complex is required for muscle fibre formation. Nat Commun. 2014; 5: 4190.